DETERMINATION OF TARGET THICKNESS OF THIN LITHIUM TARGETS

C. F. Donaghy

8854
on spine:

DONAGHY

1954

THESIS
D643

Letter on front cover:

DETERMINATION OF TARGET THICKNESS
OF THIN LITHIUM TARGETS

C. F. DONAGHY

Thesis
D643

DETERMINATION OF TARGET THICKNESS
OF THIN LITHIUM TARGETS

by

C. F. Donaghy
Lieutenant, U. S. Navy

B.S., United States Naval Academy
(1944)

SUBMITTED IN PARTIAL FULFILLMENT OF THE
REQUIREMENTS FOR THE DEGREE OF
MASTER OF SCIENCE

at the

MASSACHUSETTS INSTITUTE OF TECHNOLOGY

(1954)

Thesis
D643

DETERMINATION OF TARGET THICKNESS OF THIN LITHIUM TARGETS

C. F. Donaghy
Lieutenant, U. S. Navy

Submitted to the Department of Physics on May 24, 1954 in

partial fulfillment of the requirements for the degree of

Master of Science

ABSTRACT

A study has been made of the mechanics leading to a geometric peak in the neutron yield curve of endoergic (p,n) reactions.

Theoretical expressions have been derived for the neutron yield as a function of proton energy and counter position for the case of a monoergic proton beam, assuming isotropic emission of neutrons in the center-of-mass system and neglecting proton straggling within the target. The derivative of the theoretical yield curve is evaluated at the peak position to get an equation for target thickness in terms of peak position, counter position, and reaction threshold. These results are applied to the Li(p,n) reaction.

The effects of proton straggling and spread in the proton beam energy are then considered, and a method given to obtain an approximation to target thickness where these effects must be taken into account as is the case for very thin targets.

Thesis Supervisor: Clark Goodman

Title: Associate Professor of Physics

~~25008~~
28863

ACKNOWLEDGMENTS

The author* takes pleasure in expressing his appreciation to Dr. Robert Kiehn for suggesting this research problem and to Professor Clark Goodman, who supervised the work while in progress, for his optimism and encouragement throughout.

The author thanks Hans Mark for the many interesting discussions of this problem and related topics over the past year.

Mrs. William Guernsey and Clyde McClelland were both of material assistance in operating the generator. The unenviable task of typing the manuscript was excellently performed by Mrs. Mary E. White in a very limited amount of time, for which the author will always be grateful.

---

*Enrolled at the Massachusetts Institute of Technology under the United States Naval Postgraduate School System through the sponsorship of the Office of Naval Research.

TABLE OF CONTENTS

		Page
	List of Illustrations	ii
	List of Tables	iii
I.	INTRODUCTION	1
II.	GENERAL DISCUSSION	4
III.	CROSS SECTION	8
IV.	COUNTER SENSITIVITY	9
V.	NEUTRON YIELD	14
VI.	TARGET THICKNESS	22
VII.	PROTON ENERGY RESOLUTION	27
VIII.	THE CALIBRATED LONG COUNTER	35
IX.	THE EXPERIMENT AND RESULTS	42
X.	THE APPLICATION OF EQUATION (14)	58
XI.	CONCLUSIONS AND RECOMMENDATIONS	60
APPENDIX A:	Derivation of G, the fraction of neutrons which enter the counter	62
APPENDIX B:	Computations relative to the $Li^7(p,n)Be^7$ Reaction	69
APPENDIX C:	Possible sequences of certain defined values of the proton energy which occur when integrating over the neutron yield curve	89
BIBLIOGRAPHY		94

LIST OF ILLUSTRATIONS

		Page
Figure 1.	Target thickness versus proton energy difference between threshold and geometric peak for various effective half-angles of the long counter	25
Figure 2.	Theoretical counting rate of a calibrated long counter per unit target thickness at 1960-kev proton energy versus effective half-angle of the counter	41
Figure 3.	Neutron yield from the $Li^7(p,n)Be^7$ reaction for a 6.44-kev thick target; counter at 39.4 inches from target, on beam axis	50
Figure 4.	Neutron yield from the $Li^7(p,n)Be^7$ reaction for a 6.44-kev thick target; counter at 18.0 inches from target, on beam axis	51
Figure 5.	Neutron yield from the $Li^7(p,n)Be^7$ reaction for a 6.44-kev thick target; counter at 11.0 inches from target, on beam axis	52
Figure 6.	Neutron yield from the $Li^7(p,n)Be^7$ reaction for a 6.44-kev thick target; counter at 7.5 inches from target, on beam axis	53
Figure 7.	Effective half-angle of the long counter versus distance from the target	57
Figure 8.	Schematic representation of the mechanics of an endoergic reaction just above threshold	62a
Figure 9.	E_c versus effective half-angle of the counter	73

LIST OF TABLES

		Page
Table I (A-D)	Experimentally determined neutron yield data for a 6.44-kev thick lithium target with the long counter located at distances of 39.4, 18.0, 11.0, and 7.5 inches from the target in succession.	46 - 49
Table II	Evaluation of E_c for various effective half-angles of the counter (equations 37 and 43)	72
Table III	Evaluation of k (equation 38)	74
Table IV	Evaluation of $\frac{4(E_c - E_T)}{k^2 + 1/k^2 - 2}$ (Section VI)	75
Table V	Evaluation of K and target thickness ΔE (equation 14)	76,77
Table VI (A-C)	Evaluation of terms included in equation 30	78,79
Table VII (A-H)	Evaluation of equation 30 for various values of target thickness and half-angle of the counter	80-87
Table VIII	Theoretical relative counting rates of the long counter per unit target thickness at 1960-kev proton energy for various target thicknesses and various counter positions	88

I. INTRODUCTION

The Li(p,n) reaction has long been a source of neutrons for experimental work. In many experiments where it is necessary to know the energy resolution of the neutrons, target thickness is the main factor contributing to this resolution, and it becomes imperative to know the value of target thickness within reasonable limits. In other experiments the neutron energy resolution may be due primarily to other effects, such as energy spread of the incident proton beam or the geometry of the experiment; since the neutron energy has an angular dependence, the finite size of materials (scatterers, absorbers, and so forth) introduces a neutron energy spread. For those experiments that fall in the latter category, as is probable when using very thin targets, an accurate determination of target thickness is not important from the viewpoint of determining the neutron energy resolution. However, even here, other considerations may require that target thickness be accurately determined.

There are many articles in the literature dealing with endoergic reactions in general and the Li(p,n) reaction in particular, noteworthy among which is the work of Hansen, Taschek, and Williams[1]. As a result of their work, they observed that by using a conventional 8-inch long counter for neutron detection, located 1 meter from the target along the beam axis, the difference between the proton energy at the geometric peak and at threshold was a good approximation of target thickness. This method of determining target thickness is

commonly used and is referred to as the "rise" method. They also discussed the use of a calibrated counter for determining the thickness of fresh lithium targets.

In the course of certain experiments at this Laboratory, a question arose concerning the accuracy of the rise method of determining target thickness, and, further, the effect of moving the counter closer to the target in order to obtain higher counting rates. This thesis is the result of a study to answer the above questions. During the course of this work, it was found that target thickness had been determined previously[2,3] in at least two cases by fitting a theoretical yield curve to the experimental curve, but no thorough treatment of this method has been found. Such a method should give accurate results if the energy spread of the incident beam and straggling within the target are considered.

It would seem, however, that this method must be tedious, since two parameters, target thickness and effective half-angle of the counter, must be adjusted by trial and error until a best fit is obtained over the rise portion of the geometric peak. Whereas the shape of the rise portion of the curve and the height of the peak depend rather strongly on the proton energy spread within the target, the proton energy at which the peak occurs is not strongly dependent on the proton energy resolution. This situation is quite similar to the effect of resolution on the shape of a cross-section resonance.

It is because of this that the rise method can be used for determining the target thickness in the manner indicated in this thesis.

be represented as in Figure 8, Appendix A. The reaction is pictured as occurring at the center of sphere A, the radius (V_n) representing the velocity of the neutron in the center-of-mass system. To transform to the laboratory system, it is only necessary to add the velocity of the center of mass to each point on the surface of sphere A, thus obtaining sphere B, also of radius V_n. A vector from the center of sphere A to any point on the surface of sphere B represents a particular neutron velocity (energy) in the laboratory. Thus, a group of neutrons appears in the laboratory with essentially a continuum of velocities ranging from a minimum value ($V_{cm} - V_n$) to a maximum value ($V_{cm} + V_n$), both occurring at zero degrees.

At threshold the neutrons are "squeezed" out of the nucleus with velocity (V_n) equal to zero. In this limiting case, spheres A and B are reduced to points, and all of the neutrons appear at zero degrees in the laboratory with a velocity equal to that of the center of mass. At a slightly higher proton energy, spheres A and B have a finite size as depicted in Figure 8. Here, sphere B defines a cone of neutrons of half-angle γ. At any angle less than γ, sphere B is intercepted in two points corresponding to two different neutron energies. Consequently, an element of solid angle within the neutron cone will intercept two groups of neutrons of different energies.

Since the neutron cone is defined by the angle γ for which the cone and sphere are tangent, it follows that the point of tangency corresponds to neutrons of a particular energy.

is represented as in Figure 7, Appendix A. The direction is distinct in proportion to the radius of sphere A, the radius (V_n) representing the velocity of the neutron in the center-of-mass system. To transform to the laboratory system, it is only necessary to add the velocity of the center of mass to each point on the surface of sphere A, thus generating sphere B, also of radius V_n. A vector from the center of sphere A to any point on the surface of sphere B represents a particular neutron velocity (energy) in the laboratory. Thus, a group of neutrons appears in the laboratory with essentially a continuum of velocities ranging from a minimum value ($V_{cm} - V_n$) to a maximum value ($V_{cm} + V_n$), both occurring at zero degrees.

At threshold the neutrons are "squeezed" out of the nucleus with velocity (V_n) equal to zero. In this limiting case, spheres A and B are reduced to points, and all of the neutrons appear at zero degrees in the laboratory with a velocity equal to that of the center of mass. At a slightly higher proton energy, spheres A and B have a finite size as depicted in Figure 8. Here, sphere B defines a cone of neutrons of half-angle ψ. At any angle less than ψ, sphere B is intersected in two points corresponding to two different neutron energies. Consequently, an element of solid angle within the neutron cone will intercept two groups of neutrons of different energy.

Since the neutron cone is defined by the angle ψ for which the cone and sphere are tangent, it follows that the point of tangency corresponds to neutrons of a particular energy.

The cone gets larger with increasing proton energy until the neutron velocity in the center-of-mass system is equal to the center-of-mass velocity, at which time the cone has opened up to 2π steradians so that neutrons are being emitted into the entire forward hemisphere in the laboratory. The proton energy at which this occurs is designated E_L, and at this energy the lower-energy neutron group disappears. With any further increase of proton energy above E_L, neutrons are emitted throughout the entire 4π steradians of the laboratory.

With the long counter placed with its axis along the beam axis, the fraction (G) of neutrons emitted from thickness dE which enters the counter depends on the size of the neutron cone and the half-angle (θ) which the counter subtends at the target. If E_c is defined as that proton energy at which the neutron cone is equal to the cone subtended by the counter, then the fraction (G) has the following values (Appendix A):

$$\text{(3a)}\quad G_1 = 1 \quad . \; . \; . \; . \; . \; . \; . \; . \; . \; . \; . \; . \; . \; . \; . \; . \quad E < E_c$$

$$\text{(3b)}\quad G_2 = 1 - k\left(\frac{E - E_c}{E - E_T}\right)^{1/2} \quad . \; . \; . \; . \; . \; . \; . \; . \quad E_c < E < E_L$$

$$\text{(3c)}\quad G_3 = 1/2\left[1 - k\left(\frac{E - E_c}{E - E_T}\right)^{1/2} + b\left(\frac{E}{E - E_T}\right)^{1/2}\right] \quad . \quad E > E_L$$

where

$$k = \left(1 - \frac{m_1 m_3}{m_2 m_4}\sin^2\theta\right)^{1/2}\cos\theta = \left(\frac{E_T}{E_c}\right)^{1/2}\cos\theta$$

$$b \equiv \left(\frac{m_1 m_3}{m_2 m_4}\right)^{1/2}\sin^2\theta$$

and $m_{1,2,3,4}$ are the masses of the projectile particle, target nucleus, resultant particle, and product nucleus, respectively.

III. CROSS SECTION

From theoretical considerations, it is shown[4] that, for a neutron emitted with angular momentum ℓ, the cross section at energies just above threshold is given by:

$$\sigma_\ell\ (a,n) = \text{const}\ E_n^{\ell + 1/2} \tag{4}$$

where "a" is the charged particle inducing the reaction, and E_n is the neutron energy in the center-of-mass system. Because of the high centrifugal barrier in the region just above threshold for neutrons with angular momentum other than zero[5], the contribution to the yield from such neutrons will be small compared with that from neutrons having zero angular momentum, hence no centrifugal barrier.

Since the threshold neutrons mostly have $\ell = 0$,

$$\sigma\ (a,n) = \text{const}\ E_n^{1/2} = \text{const}\ V_n. \tag{5}$$

In Appendix A, it is shown that the neutron velocity in the center-of-mass system is given by:

$$V_n = \text{const}\ (E - E_T)^{1/2}$$

where E_T is the threshold energy and E the instantaneous energy of the incident particle. Then the cross section σ may be written:

$$\sigma = C(E - E_T)^{1/2} \quad \text{where C is a constant.} \tag{6}$$

IV. COUNTER SENSITIVITY

The 8-inch long counter[6] is the result of several attempts to find an arrangement of paraffin surrounding a boron detector such that the number of boron disintegrations is proportional to the number of primary-source neutrons and independent of their energies over a wide range. This counter consists of a paraffin cylinder 12 inches in length and 8 inches in diameter. Along its axis is a BF_3 proportional counter 1 inch in diameter and 8 inches in active length is embedded. It protrudes slightly over the front face of the paraffin but is protected from direct thermal neutrons by a cadmium shield. An aluminum tube shields the counter electrically. For insulation, the space between the counter wall and the shield is filled with ceresin wax. The central electrode consists of a Kovar wire of 10-mil diameter. The counter is filled with enriched (80 percent B^{10}) BF_3 to a pressure of 25 cm Hg. With -2700 volts applied to the wall a gas multiplication of about 10 is obtained. With the source of neutrons placed on the counter axis one meter from the face, a flat response is obtained in the region from about 0.5 to 3.0 Mev. The performance of the counter may be explained qualitatively as follows.

The length of the counter is many times greater than the mean free path of any neutrons to be detected. Neutrons entering the paraffin are degraded to thermal energies and diffuse into the detector where they give rise to $B(n,\alpha)$ reactions. Because of the large

cross section, the counting rate is determined essentially by the flux of thermal neutrons. For an infinitely large slab of paraffin, the efficiency would increase with increasing neutron energy, since low-energy neutrons penetrate only a short distance into the paraffin before being thermalised. Therefore, the low-energy neutrons have a better chance of escaping through the front face (instead of passing through the detector) than neutrons that were originally of higher energy and are thermalized at a greater distance from the front face. There are two reasons for this. At higher energies, more collisions are required for thermalization, and the collision cross section is smaller than at low energies. In order to minimize the dependence of the efficiency on the energy, the dimensions of the paraffin must be such that the thermalized fast neutrons have an increased chance to escape from the paraffin.

The probability that a neutron striking a long counter will be counted is a function of its energy and direction, and the distance from the counter axis at which it strikes. The conventional 8-inch long counter has been designed to give a flat response in the region from about 0.5 to 3 Mev, for a uniform distribution over the face of the counter. The situation is somewhat different in this problem as the neutrons are emitted in a cone of varying solid angle within which the energy distribution is not uniform. Only after the cone has opened up to 4π steradians is the distribution approximately uniform over the counter face, but the forward direction is still favored.

A theoretical calculation of counter sensitivity would be very difficult, if not impossible. It seems that the best solution to the problem is to consider counter sensitivity as being constant, and to use a counter which is modified to best satisfy this assumption consistent with reasonable yield.

For proton energies up to 40 kev above threshold, neutron energies will range from a few kev to about 120 kev. (Figure 13 of reference 1.) For each proton energy in this range, the counter will intercept all of the neutrons if $E < E_c$ or two groups, high and low energy, if $E > E_c$. Because of the finite thickness of the target, both situations can occur simultaneously. The net result is that neutrons of various energies are incident upon the counter for any proton energy.

The experimental sensitivity curves of Hanson and McKibben[6] show that a 6-inch paraffin diameter gives a flatter response than the conventional 8-inch counter for neutrons in the energy range from thermal to a few hundred kev. This is explained by the fact that the sensitivity of the counter to high-energy neutrons is decreased because of the smaller mass of paraffin, and the sensitivity to low-energy neutrons is therefore relatively high. It may be inferred that a paraffin diameter less than 6 inches will give a still flatter response over the energy range of interest. Snowden and Whitehead[2] have used a 4-inch paraffin diameter in their work of fitting a theoretical yield curve to the experimental yield curve.

R. A. Nobles et al[7] have modified the shielded long counter[6] by employing a BF_3 counter of larger diameter placed slightly farther forward in the paraffin moderator. Whereas the conventional shielded long counter shows a 10 percent drop in efficiency at 25 kev compared to the flat response region, it is claimed for the modified counter that no decrease in efficiency has occurred at 25 kev.

In the design of the optimum counter, another factor must be considered. Those neutrons which strike near the outer periphery of the paraffin have a velocity which is at an angle with respect to the counter axis. This may be represented as follows:

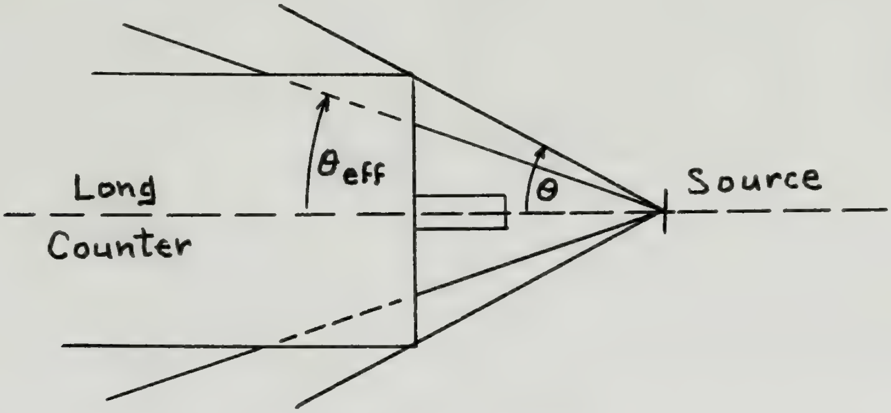

These neutrons have a higher probability of escaping from the counter because of the smaller amount of paraffin in the direction of their motion. The result is that the counter will have an effective half-angle (θ_{eff}) less than its true half-angle (θ). This effect is increased as the counter is moved closer to the target. It seems that

A. L. Fiedler et al[7] have modified the collimator they employed[8] by employing a [illegible] of larger diameter [illegible] slightly tapered forward to the straight collimator. Because the conventional [illegible] long counter shows a 10 percent drop in efficiency at [illegible] Mev compared to the flat response region, it is claimed for the modified counter that no decrease in efficiency has occurred at 15 Mev.

In the design of the neutron counter, another factor must be considered. Those neutrons which strike near the outer periphery of the counter have a velocity which is at an angle with respect to the counter axis. This may be represented as follows:

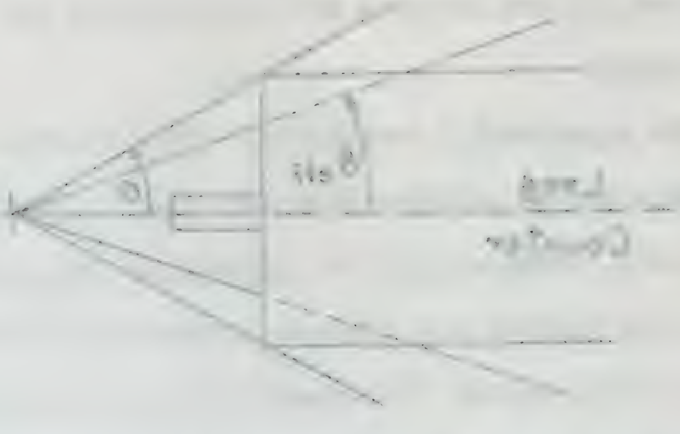

These neutrons have a higher probability of escaping from the counter because of the smaller amount of paraffin in the direction of their motion. The result is that the counter will have an effective half-angle (θ_{eff}) less than the true half-angle (θ). This effect is increased as the counter is moved closer to the target. It seems that the use of a truncated cone of paraffin as employed by Bonner and Butler[3] would reduce this effect. However, for optimum results, this would demand a separate truncated cone for each position of the counter. Even then, one could not expect the loss of counts to occur sharply at $E = E_c$. Possibly the best practical counter would be one having a truncated cone corresponding to the average position at which the counter is expected to be used.

The benefits of such an optimum design may not be sufficient to offset the advantage of using the conventional counter. In either case, it will be necessary to know the effective half-angle of the counter for various counter positions.

V. NEUTRON YIELD

Letting ϵ = constant and $\sigma = C(E - E_T)^{1/2}$ in accordance with the foregoing discussions, equation (2) becomes:

$$N_c = Z \int_{E_o-\Delta E}^{E_o} G\,(E - E_T)^{1/2}\, dE \tag{7}$$

where $Z \equiv N\,n\,f\,\epsilon\,C$ = a constant, and ΔE = target thickness.

Equations (3a,b,c) indicate that the form of the analytical expression defining G depends on the value of E at the point in question. This causes the integral of equation (7) to break up into two integrals if at any point within the target the proton energy has the value E_c or E_L. In order to evaluate equation (7) over the yield curve from threshold to a point beyond the geometric peak, it is necessary to know the sequence of E values. Only then can the proper G value and the limits of integration be correctly selected. Of the five possible sequences of E values discussed in Appendix B, it is there shown that only the following two sequences can occur for counter half-angles less than 30 degrees and target thicknesses less than 30 kev. (These two sequences are arranged in order of increasing E and will hereafter be referred to as cases I and II):

I	II
E_T	E_T
E_c	$E_T + \Delta E$
$E_T + \Delta E$	E_c
$E_c + \Delta E$	$E_c + \Delta E$
E_L	E_L
$E_L + \Delta E$	$E_L + \Delta E$

For target thicknesses up to $(E_L - E_T)/2$ (19.85 kev for lithium), case I will occur for $E_c < (E_T + \Delta E)$ and case II for $E_c > (E_T + \Delta E)$. Only case I can occur for

$$\left(\frac{E_L - E_T}{2}\right) < \Delta E < (E_L - E_c)$$

which for lithium is: 19.85 kev $< \Delta E <$ 30 kev.

These two sequences may be illustrated in a typical situation as follows:

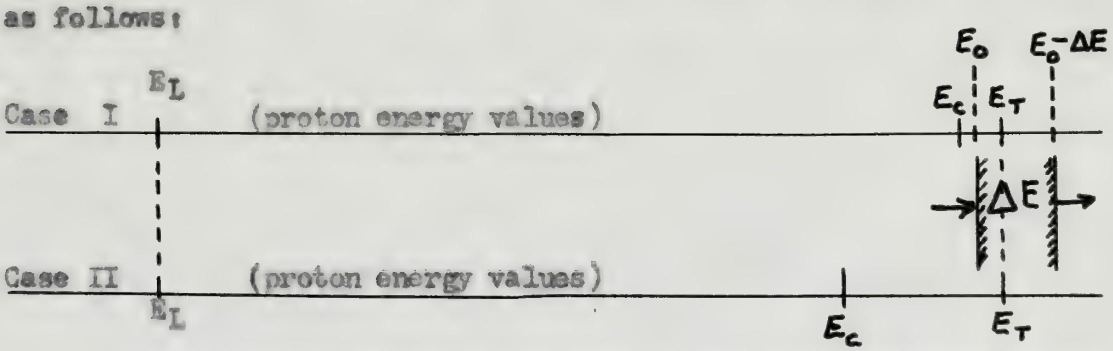

As the proton energy scales move to the right relative to the target of thickness ΔE, they indicate the manner in which the various

integrals arise when integrating over the yield curve. Expressing this mathematically, equation (7) takes the forms:

Case I: Nc/Z equals

$$\int_{E_T}^{E_o} G_1 \sigma \, dE \quad . \; . \; . \; . \; . \; . \; . \; . \; . \; . \quad E_T < E_o < E_c \tag{8a}$$

$$\int_{E_T}^{E_c} G_1 \sigma \, dE + \int_{E_c}^{E_o} G_2 \sigma \, dE \quad . \quad E_c < E_o < E_T + \Delta E \tag{8b}$$

$$\int_{E_o-\Delta E}^{E_c} G_1 \sigma \, dE + \int_{E_c}^{E_o} G_2 \sigma \, dE \quad . \; . \quad E_T+\Delta E < E_o < E_c+\Delta E \tag{8c}$$

$$\int_{E_o-\Delta E}^{E_o} G_2 \sigma \, dE \quad . \; . \; . \; . \; . \; . \; . \; . \; . \; . \; . \quad E_c+\Delta E < E_o < E_L \tag{8d}$$

$$\int_{E_o-\Delta E}^{E_L} G_2 \sigma \, dE + \int_{E_L}^{E_o} G_3 \sigma \, dE \quad . \; . \quad E_L < E_o < E_L+\Delta E \tag{8e}$$

$$\int_{E_o-\Delta E}^{E_o} G_3 \sigma \, dE \quad . \; . \; . \; . \; . \; . \; . \; . \; . \; . \; . \; . \quad E_o > E_L+\Delta E \tag{8f}$$

Case II: Nc/Z equals

$$(9a)\quad \int_{E_T}^{E_o} G_1\,\sigma\,dE \quad \ldots\ldots\ldots\ldots \quad E_T < E_o < E_T+\Delta E$$

$$(9b)\quad \int_{E_o-\Delta E}^{E_o} G_1\,\sigma\,dE \quad \ldots\ldots\ldots\ldots \quad E_T+\Delta E < E_o < E_c$$

$$(9c)\quad \int_{E_o-\Delta E}^{E_c} G_1\,\sigma\,dE + \int_{E_c}^{E_o} G_2\,\sigma\,dE \quad \ldots \quad E_c < E_o < E_c+\Delta E$$

(9d,e,f) These are identical to (8d,e,f), respectively.

It is seen from equations (3a,b,c) that $G\,\sigma$ has the values:

$$G_1\,\sigma = (E - E_T)^{1/2}$$

$$G_2\sigma = (E - E_T)^{1/2} - k(E - E_c)^{1/2} = G_1\,\sigma - k(E - E_c)^{1/2}$$

$$G_3\,\sigma = 1/2 \quad (E - E_T)^{1/2} - k(E - E_c)^{1/2} + b\,E^{1/2}$$

$$= 1/2 \quad G_2\,\sigma + b\,E^{1/2}$$

Substituting these expressions for $G_{1,2,3}\,\sigma$ in equations (8) and (9) gives:

Case I: Nc/Z equals

$$(10a) \int_{E_T}^{E_o} (E - E_T)^{1/2}\, dE \quad \ldots\ldots\ldots\ldots \quad E_T < E_o < E_c$$

$$(10b) \int_{E_T}^{E_o} (E - E_T)^{1/2} dE - k\int_{E_c}^{E_o} (E - E_c)^{1/2} dE \quad . \quad E_c < E_o < E_T+\Delta E$$

$$(10c) \int_{E_o-\Delta E}^{E_o} (E - E_T)^{1/2} dE - k\int_{E_c}^{E_o} (E - E_c)^{1/2} dE \quad . \quad E_T+\Delta E < E_o < E_c+\Delta E$$

$$(10d) \int_{E_o-\Delta E}^{E_o} \left[(E - E_T)^{1/2} - k(E - E_c)^{1/2}\right] dE \quad \ldots\ldots \quad E_c+\Delta E < E_o < E_L$$

$$(10e) \int_{E_o-\Delta E}^{E_o} \left[(E - E_T)^{1/2} - k(E - E_c)^{1/2}\right] dE - 1/2\int_{E_L}^{E_o} \left[(E - E_T)^{1/2}\right.$$

$$\left. - k(E - E_c)^{1/2} - b\, E^{1/2}\right] dE \quad \ldots \quad E_L < E_o < E_L+\Delta E$$

$$(10f)\ 1/2\int_{E_o-\Delta E}^{E_o} \left[(E - E_T)^{1/2} - k(E - E_c)^{1/2} + b\, E^{1/2}\right] dE \qquad E_o > E_L+\Delta E$$

Case II: Nc/Z equals

$$(11a) \int_{E_T}^{E_o} (E - E_T)^{1/2}\, dE \quad . \; . \; . \; . \; . \; . \; . \; . \quad E_T < E_o < E_T + \Delta E$$

$$(11b) \int_{E_o - \Delta E}^{E_o} (E - E_T)^{1/2}\, dE \quad . \; . \; . \; . \; . \; . \; . \quad E_T + \Delta E < E_o < E_c$$

$$(11c) \int_{E_o - \Delta E}^{E_o} (E - E_T)^{1/2}\, dE - k \int_{E_c}^{E_o} (E - E_c)^{1/2}\, dE \; . \; E_c < E_o < E_c + \Delta E$$

(11d,e,f) These are identical to (10d,e,f), respectively.

Integration of equations (10) and (11) give the following expressions:

Case I: $3Nc/2Z$ equals

(12a) $(E_o - E_T)^{3/2}$ . . . . $E_T < E_o < E_c$

(12b) $(E_o - E_T)^{3/2} - k(E_o - E_c)^{3/2}$. . . . . $E_c < E_o < E_T + \Delta E$

(12c) $(E_o - E_T)^{3/2} - (E_o - E_T - \Delta E)^{3/2} - k(E_o - E_c)^{3/2}$. $E_T + \Delta E < E_o < E_c + \Delta E$

(12d) $(E_o - E_T)^{3/2} - (E_o - E_T - \Delta E)^{3/2} - k\left[(E_o - E_c)^{3/2} - (E_o - E_c - \Delta E)^{3/2}\right]$

. . . . $E_c + \Delta E < E_o < E_L$

(12e) $1/2\Big\{(E_o - E_T)^{3/2} - 2(E_o - E_T - \Delta E)^{3/2} + (E_L - E_T)^{3/2} + b(E_o^{3/2} - E_L^{3/2})$

$-k\left[(E_o - E_c)^{3/2} - 2(E_o - E_c - \Delta E)^{3/2} + (E_L - E_c)^{3/2}\right]\Big\}$ $E_L < E_o < E_L + \Delta E$

(12f) $1/2\Big\{(E_o - E_T)^{3/2} - (E_o - E_T - \Delta E)^{3/2} + b\left[E_o^{3/2} - (E_o - \Delta E^{3/2})\right]$

$-k\left[(E_o - E_c)^{3/2} - (E_o - E_c - \Delta E)^{3/2}\right]\Big\}$. . . . $E_o > E_L + \Delta E$

Case II: $3Nc/2Z$ equals

(13a) $(E_o - E_T)^{3/2}$ . . . . $E_T < E_o < E + \Delta E$

(13b) $(E_o - E_T)^{3/2} - (E_o - E_T - \Delta E)^{3/2}$ . . . . $E_T + \Delta E < E_o < E_c$

(13c) $(E_o - E_T)^{3/2} - (E_o - E_T - \Delta E)^{3/2} - k(E_o - E_c)^{3/2}$. $E_c < E_o < E_c + \Delta E$

(13d,e,f) These are identical to (12d,e,f), respectively.

These equations may be used for computing a theoretical yield curve. A word of caution must be injected at this point concerning equations (12e,f) and (13e,f). These have been derived from the assumption that $\sigma = C(E - E_T)^{1/2}$, and they will prove useful for reactions where that assumption is valid for the regions in question. The cross section for the Li(p,n) reaction, however, is almost constant throughout portions of the regions to which these equations apply. This is no handicap, however, since the equations (12a-d) and (13a-d) enable one to compute a theoretical yield curve for target thicknesses up to 30 kev which is the limit of thickness being considered.

VI. TARGET THICKNESS

A visual inspection of equations (12a,b) and (13a,b) shows that the geometric peak must occur for:

Case I: $E_o > E_T + \Delta E$

Case II: $E_o > E_c$

The requirement that the peak occur in the region defined by equations (12c) and (13c) for Cases I and II, respectively, is in either case:

$$N_c(\text{at } E_o = E_c + \Delta E - \epsilon) > N_c(\text{at } E_o = E_c + \Delta E)$$

where ϵ is an infinitesimal.

Utilizing equation (12c) or (13c), the requirement is:

$$(E_c - E_T + \Delta E - \epsilon)^{3/2} - (E_c - E_T - \epsilon)^{3/2} - k(\Delta E - \epsilon)^{3/2} >$$

$$(E_c - E_T + \Delta E)^{3/2} - (E_c - E_T)^{3/2} - k(\Delta E)^{3/2}$$

Expanding and collecting terms:

$$3/2 \quad \epsilon \left[(E_c - E_T)^{1/2} - (E_c - E_T + \Delta E)^{1/2} + k(\Delta E)^{1/2} \right] > 0$$

$$(E_c - E_T)^{1/2} + k(\Delta E)^{1/2} > (E_c - E_T + \Delta E)^{1/2}$$

Squaring both sides:

$$k^2\Delta E \;+\; 2k(\Delta E)^{1/2}(E_c - E_T)^{1/2} \;>\; \Delta E$$

$$\left(\frac{1 - k^2}{2k}\right)^2 \Delta E \;<\; E_c - E_T$$

$$\Delta E \;<\; \frac{4(E_c - E_T)}{k^2 + 1/k^2 - 2}$$

Evaluation of the expression on the right-hand side of this inequality (Table IX, Appendix B) for values of θ between zero and 30 degrees, shows that this inequality holds for target thicknesses up to about 400 kev. Thus, the peak will occur in the regions defined by equations (12c) and (13c) for Cases I and II, respectively. Taking the derivative of N_c with respect to E_o in this region and evaluating at the peak position:

$\left.\frac{dN_c}{dE_o}\right|_{E_p}$ = 0, where E_p is the incident particle energy at the peak position.

$$(14) \qquad \Delta E = E_p - E_T - K$$

where

$$K \equiv \left[(E_p - E_T)^{1/2} - k(E_p - E_c)^{1/2} \right]^2$$

$$\equiv \left[(E_p - E_T)^{1/2} - \cos\theta\, E_T^{1/2} (\frac{E_p}{E_c} - 1)^{1/2} \right]^2$$

The correction term (K) and the target thickness (ΔE) are evaluated in Table X for various values of the effective half-angle of the counter (θ_{eff}), and the proton energy difference between the geometric peak and the reaction threshold ($E_p - E_T$). The results are presented as a family of curves in Figure 1.

If one assumes that the cross section is given by:

$$(15) \qquad \sigma = \text{const} \, (\frac{E - E_T}{E^5})^{1/2}$$

Or, equally well, if one introduces the slowly varying constant $1/E^{5/2}$ under the integral sign of equations (10) and (11), then integration of these equations gives results that can be shown to be identical to the expressions given by Snowden and Whitehead[2] for Case I; they have made no mention of Case II. Proceeding as above, the derivative in the region of the peak leads to:

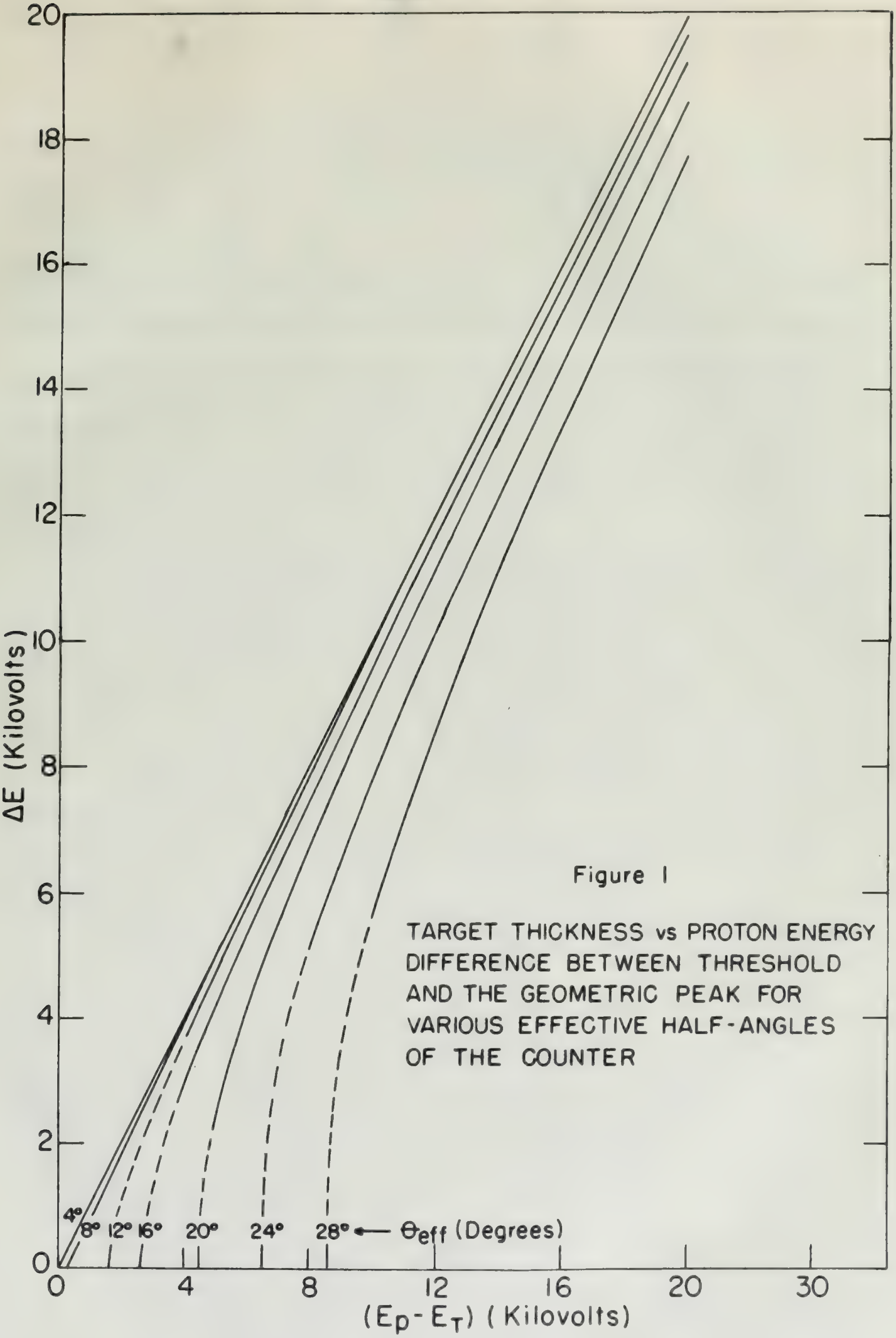

Figure 1

TARGET THICKNESS vs PROTON ENERGY DIFFERENCE BETWEEN THRESHOLD AND THE GEOMETRIC PEAK FOR VARIOUS EFFECTIVE HALF-ANGLES OF THE COUNTER

$$(16) \qquad \Delta E \simeq \frac{E_p - E_T - K}{1 - 5K/E_p} \simeq E_p - E_T - K$$

in close agreement with equation (14). This is not surprising, since there is but little variation in the factor ($1/E^{5/2}$) over the relatively small range of energy being considered. Since these results add nothing new to the results previously obtained, the rather lengthy manipulations required for confirmation of the statements just made are omitted.

Equation (14) reduces to the result given by Hanson, Taschek, and Williams[1] when θ is small, namely:

$$(17) \qquad \Delta E \simeq E_p - E_T.$$

VII. PROTON ENERGY RESOLUTION

The result arrived at in equation (14) is based upon the assumption of an incident monergic proton beam with no proton straggling within the target. The effects will now be considered of an initial energy spread and straggling within the target.

The Rockefeller generator has an effective energy spread of about 0.075 percent with the entrance and exit slits set at 1.0 mm width[8]. Several microamperes of beam current are available with this energy definition. Better energy resolution may be obtained at the expense of beam current by using a narrower slit width.

In order to calculate the straggling it is necessary to know the stopping power (energy loss per unit weight per unit area). Bethe's[9,10] treatment of energy loss, based upon the Born approximation, after correction for K shell binding, leads to the following equation in the nonrelativistic case:

$$(18) \qquad -\frac{dE}{dX} = \frac{4\pi e^4 z^2 N}{mv^2} \left[Z \, \ell n \left(\frac{2\,mv^2}{I} \right) - C_k \right]$$

where

ze = charge of the incident particle

v = velocity of the incident particle

Z = the nuclear charge of the material

m = electronic mass

I = average excitation potential of the atom

N = number of atoms per cm^3 of the material

C_k = correction term to account for binding in K shell.

This equation as it stands gives the energy loss per unit path length. This equation is used to obtain the stopping power of lithium relative to beryllium for which the absolute value of stopping power is well known[10]. This immediately gives:

$$(19) \qquad \frac{-\frac{dE}{d(\rho X)_{Li}}}{-\frac{dE}{d(\rho X)_{Be}}} = \frac{W_o \left[Z \ \ell n \left(\frac{2mv^2}{I}\right) - C_k \right]}{W \left[Z_o \ \ell n \left(\frac{2mv^2}{I_o}\right) - C_{k_o} \right]} = 1.09$$

where ρ = density, W = atomic weight, and the subscript "o" denotes the standard which in this case is beryllium. The calculation follows:

$$\text{Relative stopping power} = \frac{B/W}{B_o/W_o}$$

where B and B_o are the quantities within the brackets of numerator and denominator, respectively.

$$2mv^2 = \left(\frac{4m}{M}\right)\left(\frac{Mv^2}{2}\right) = \frac{E_p}{459}$$

where M and E_p are the mass and energy of the proton, respectively.

Taking $E_p = 1900$ kev $= 1.9 \times 10^6$ ev,

$$\ell n\left(\frac{E_p}{459}\right) = \ell n \ 4139 = 8.324$$

$$\ell n \; I = \ell n \; 34 = 3.526$$

$$\ell n \; I_o = \ell n \; 60.4 = 4.101$$

The above I values are from Table 4, reference (9).

$$C_k \simeq C_{k_o} = 0.405 \quad \text{(Table II-1, reference (10))}.$$

Therefore,

$$\frac{B}{B_o} = \frac{14.394 - 0.405}{16.892 - 0.405} = 0.8485.$$

$$\text{Rel. Stop. Pwr (Li to Be)} = \frac{W_o}{W} (0.8485) = \frac{9.015}{7.018} (0.8485) = 1.09$$

Using the value 144 for the absolute stopping power of beryllium for 1900-kev protons (Table III-7, reference (10)), one obtains for lithium:

$$\text{Stopping Power (Li)} = 144 \times 1.09 = 157 \; \frac{\text{kev cm}^2}{\text{mg}}$$

An initially homogeneous beam of protons, after passing through a target of thickness t will have an energy distribution with a standard deviation Ω given by[11]:

(20) $$\Omega^2 = \frac{4\pi e^4}{M}\left(\frac{Z}{A}\right) t$$

where M and e are the mass and charge of the proton, Z and A are the atomic and mass numbers of the target element, respectively. The thickness t is in weight per unit area.

(21) $$\Omega = \sqrt{\frac{2\pi e^4}{M}}\left(\frac{2Z}{A}\right)^{1/2} t^{1/2} = 8.85\left(\frac{2Z}{A}\right)^{1/2} t^{1/2}$$

where $\frac{2Z}{A} \simeq 1$ for all elements except hydrogen.

$$\frac{2Z}{A}\text{ (lithium)} = \left(\frac{6}{7}\right)^{1/2} \simeq 0.93.$$

(22) $\Omega = 8.23\ t^{1/2}$ for lithium; where Ω is given in kev, and t is in mg/cm^2.

Since the stopping power of lithium was calculated to be

$$157\ \frac{\text{kev cm}^2}{\text{mg}}$$

we may write:

(23) $\Omega = 0.657\ (\Delta E)^{1/2}$ where Ω is in kev and ΔE is the target thickness in kev. From this equation, the following table is computed:

ΔE(kev)	(kev)	$2\Gamma_s$(kev)
20	2.94	6.94
15	2.54	5.98
10	2.08	4.90
5	1.47	3.46
4	1.31	3.09
3	1.14	2.69
2	0.93	2.19
1	0.66	1.55
0.5	0.46	1.08

Assuming a normal distribution, the half-width at half maximum (Γ_s) is given by:

$$\Gamma_s = 1.178\,\Omega = 0.774\,(\Delta E)^{1/2}.$$

The value of $2\Gamma_s$ is given in the above table for ready comparison with the proton energy spread of the beam, which is about 1.4 kev, for an 0.075 percent energy definition.

It is now desired to determine the minimum value of target thickness for which equation (14) may be expected to be valid when threshold is to be determined by extrapolating the linear portion of the yield curve to the axis. It is unlikely that a precise theoretical treatment can be given. However, an approximate value for this

minimum thickness may be obtained by qualitative arguments based upon some rather crude assumptions, in the following manner.

The geometric peak is treated as a resonance peak with full width at half maximum of the order of 1.4 $(E_p - E_T)$. It is shown (Section 3D of reference (9)) that for a resolution equal to or less than the width of half maximum of the resonance peak, the main effect is to depress the peak without changing the slope of the linear portion of the curve. Applying this condition to the geometric peak for a resolution of 2 Γ, it follows that for

$$\Gamma < 0.7\ \Delta E < 0.7(E_p - E_T)$$

extrapolation to the axis of the linear portion of the rise curve should still give a good value of the reaction threshold. Although the peak has been depressed, there will be no appreciable shift in peak position, inasmuch as the geometric peak is only slightly asymmetrical. Thus, the value of $(E_p - E_T)$ obtained by extrapolation is essentially the same value as would have been obtained with no resolution, and equation (14) will be valid.

The resolution (2 Γ) used in the foregoing discussion is the resultant of energy spread in the beam and straggling in the target and will be of the order of the larger of these two resolutions, considered separately. A slightly better value is obtained if it is assumed that these two resolutions add as Gaussians:

$$\Gamma^2 = \Gamma_s^2 + \Gamma_i^2$$

where Γ_i is the half-width at half maximum of the energy distribution in the beam. Actually, the shape of the energy distribution in the beam is largely dependent upon the exit slit width of the magnetic analyzer (private communication with W. M. Preston), departing from an approximate Gaussian as the slit width is decreased.

Applying the foregoing results to the specific case of a 2-kev target thickness and a 1-mm slit width gives:

$$2\Gamma = \left[(2.19)^2 + (1.4)^2\right]^{1/2} = 2.6 \text{ kev.}$$

Since $\Gamma = 1.3$ kev, the condition for validity of equation (14)

$\Gamma < 0.7\ \Delta E$ becomes

$\Gamma < 1.4$ kev,

and this inequality holds for the conditions stated.

The conclusion to be drawn from the foregoing is that equation (14) will be valid for target thicknesses of about 2 kev minimum, when the threshold is determined by extrapolation and slit widths of 1 mm are used on the Rockefeller generator.

For $\Gamma > 0.7\ (E_P - E_T)$, extrapolation to the axis gives an apparent threshold energy E_T' which is less than E_T since the slope of the curve is decreased. Assuming that the peak position is not

shifted because of resolution, equation (14) becomes:

$$(25) \qquad \Delta E = E_p - E_T - K = E_p - E_T' - K - \delta E_T$$

where δE_T is the difference between the true and apparent threshold. This could be determined experimentally for various values of resolution and target thickness. It is apparent, however, that equation (14) may still be used with reasonable results if the position of E_T is accurately known. An accurate method for determining the absolute value of E_T is to measure the yield over the "rise" portion of the geometric peak of a target which is several times thicker than the proton energy resolution of the beam ($\Delta E \sim 20$ kev), using an effective half-angle of the counter, such that $E_c - E_T \sim 4$ kev. Equation (13a) then applies over the lower portion of the curve where the shape is not affected by the relatively small resolution.

$$N_c \propto (E_o - E_T)^{3/2}$$

A plot of $N_c^{2/3}$ should thus be linear and its extrapolation to the axis should give an accurate value of E_T. The extreme lower portion of the yield curve must of course be neglected as it has been distorted by the incident proton energy spread.

VIII. THE CALIBRATED LONG COUNTER

The use of a calibrated long counter for determining the thickness of lithium targets is mentioned by Hanson, Taschek, and Williams[1]. Aging of the target caused by oxidation, contamination, and the like causes the geometric peak to shift toward higher proton energies, since the total number of atoms has increased. However, the yield at proton energies well above threshold is essentially the same for either the fresh or the aged target, since the number of lithium atoms has not changed while the geometric effects tend to disappear with increasing proton energy. This is attributed to the fact that at proton energies greater than E_L, the neutrons are emitted more nearly isotropically in the laboratory, and the distribution of neutron energies is more nearly uniform over the face of the counter. The change in the shape of the yield curve as a target ages is clearly shown in Figure 17 of reference (1).

It is important to note that target thickness as obtained by a calibrated counter may be used for determining the number of target atoms for either a fresh or aged target. However, the target thickness for purposes of determining the neutron resolution (arising from this target thickness) can be obtained with a calibrated counter only for a fresh target. Conversely, the "rise" method gives target thickness for purposes of determining the neutron resolution (arising from target thickness) for both fresh or aged targets; whereas it leads

to a determination of the number of target (lithium) atoms only for fresh targets. Hence, the necessity of using fresh targets is apparent when one desires to calibrate a counter in terms of counting rate per unit target thickness, if thickness is determined by the rise method for the purpose of calibration.

A measurement of the thickness of a fresh target by the "rise" method followed by a measurement of the yield at a proton energy above 1930 kev in a region where the cross section is nearly constant serves to calibrate the counter in terms of counting rate per unit target thickness. One may select a region of nearly constant cross section either above or below the 2.24-Mev resonance. The region above the peak should give better results as the geometric effect is less pronounced than in the region below the peak.

A calculation will be made to determine the linearity of neutron yield with respect to target thickness for various counter positions for an incident proton energy (E_0) of 1960 kev. This particular value is selected not only because the cross section will be nearly constant for all possible E values within targets of thickness 0 to 30 kev, but also because equation (8f) will apply throughout since $E > E_L$ for all possible E values within the target.

$$(8f) \qquad N_0 = Z \int_{E_0-\Delta E}^{E_0} G_3 \, \sigma \, dE \;.\;.\;.\;.\;.\;. \qquad E > E_L$$

and since σ is nearly constant:

$$N_c = Z\sigma \int_{E_o-\Delta E}^{E_o} G_3 \, dE. \tag{26}$$

As the proton energy increases, G_3 approaches a limit which is constant for a given half-angle of the counter. Thus, the counting rate (N_c) approaches ($\sigma Z\ G_3$) ΔE = const ΔE.

If, however, we evaluate N_c at E_o = 1960 kev,

$$N_c = \frac{\sigma Z}{2} \int_{E_o-\Delta E}^{E_o} \left[1 - \cos\theta \left\{ 1 - \frac{m_1 m_3}{m_2 m_4} \sin^2\theta \left(\frac{E}{E - E_T} \right) \right\}^{1/2} + \sin^2\theta \left(\frac{m_1 m_3}{m_2 m_4} \right)^{1/2} \left(\frac{E}{E - E_T} \right)^{1/2} \right] dE \tag{27}$$

Another form of the expression for G_3 is used here (equation 36c of Appendix A):

$$\frac{m_1 m_3}{m_2 m_4} \sim 0.02 \qquad (\sin\ \theta)^2_{max} \sim 0.25 \qquad \frac{E}{E - E_T} \sim 25$$

Therefore:

$\left[\frac{m_1 m_3}{m_2 m_4} \sin^2\theta \left(\frac{E}{E - E_T}\right)\right]_{\max} \sim$ 0.125; hence, only two terms are needed in the series expansion of the brackets containing this factor:

$$(28) \qquad N_c = \frac{\sigma Z}{2}\left[(1 - \cos\theta)\int_{E_o-\Delta E}^{E_o} dE + \frac{\cos\theta \sin^2\theta}{2}\left(\frac{m_1 m_3}{m_2 m_4}\right)\int_{E_o-\Delta E}^{E_o} \frac{E}{E - E_T}\, dE\right.$$

$$\left. + \sin^2\theta \left(\frac{m_1 m_3}{m_2 m_4}\right)^{1/2}\int_{E_o-\Delta E}^{E_o}\left(\frac{E}{E - E_T}\right)^{1/2} dE\right]$$

First integral:

$$\int_{E_o-\Delta E}^{E_o} dE = \Delta E$$

Second integral:

$$\int_{E_o-\Delta E}^{E_o} \frac{E}{E - E_T}\, dE = \Big[E + E_T \ln(E - E_T)\Big]_{E_o-\Delta E}^{E_o} = \Delta E + E_T \ln\left[\frac{E_o - E_T}{E_o - E_T - \Delta E}\right]$$

Third integral:

$$\int_{E_o-\Delta E}^{E_o} \left(\frac{E}{E - E_T}\right)^{1/2} dE = E_o^{1/2} \int \frac{dE}{(E - E_T)^{1/2}}$$ since $E^{1/2}$ is

nearly constant over the range of integration. This is readily integrated:

$$E_o^{1/2}\int_{E_o-\Delta E}^{E_o} \frac{dE}{(E - E_T)^{1/2}} = 2E_o^{1/2} (E - E_T)^{1/2} \Big|_{E_o-\Delta E}^{E_o}$$

$$= 2E_o^{1/2} \left[(E_o - E_T)^{1/2} - (E_o - E_T - \Delta E)^{1/2}\right]$$

Neglecting all terms except the first two in the expansion of $\left[(E_o - E_T) - \Delta E\right]^{1/2}$, one obtains:

$$\int_{E_o-\Delta E}^{E_o} \frac{E^{1/2}}{(E - E_T)^{1/2}} dE \cong \frac{\Delta E}{(1 - E_T/E_o)^{1/2}}$$

$$(29)\ N_c = \frac{\sigma Z}{2} \left\{ \left[1 - \cos\theta + \frac{\cos\theta \sin^2\theta}{2} \left(\frac{m_1 m_3}{m_2 m_4}\right) + \left(1 - \frac{E_T}{E_o}\right)^{-1/2} \sin^2\theta \left(\frac{m_1 m_3}{m_2 m_4}\right)^{1/2} \right] \Delta E + \frac{\cos\theta \sin^2\theta}{2} \left(\frac{m_1 m_3}{m_2 m_4}\right) E_T \ \ell n \left[\frac{E_o - E_T}{E_o - E_T - \Delta E} \right] \right\}$$

$$(30)\ N_c = \frac{\sigma Z}{2} \left\{ \left[1 - \cos\theta + 0.01032 \cos\theta \sin^2\theta + 0.71850 \sin^2\theta \right] \Delta E + 19.385 \ \ell n \left(\frac{78}{78 - \Delta E} \right) \cos\theta \sin^2\theta \right\}$$

Equation (30) is evaluated for various θ and various ΔE in Tables VI through VIII, the final results being displayed in Table VIII. From this table, it is seen that the counting rate per unit target thickness is practically constant for any given half-angle of counter. The results expressed in Table VIII are plotted to give the curve of Figure 2. The linearity of counting rate with respect to target thickness for a given half-angle of the counter is displayed in Tables VII (A-H).

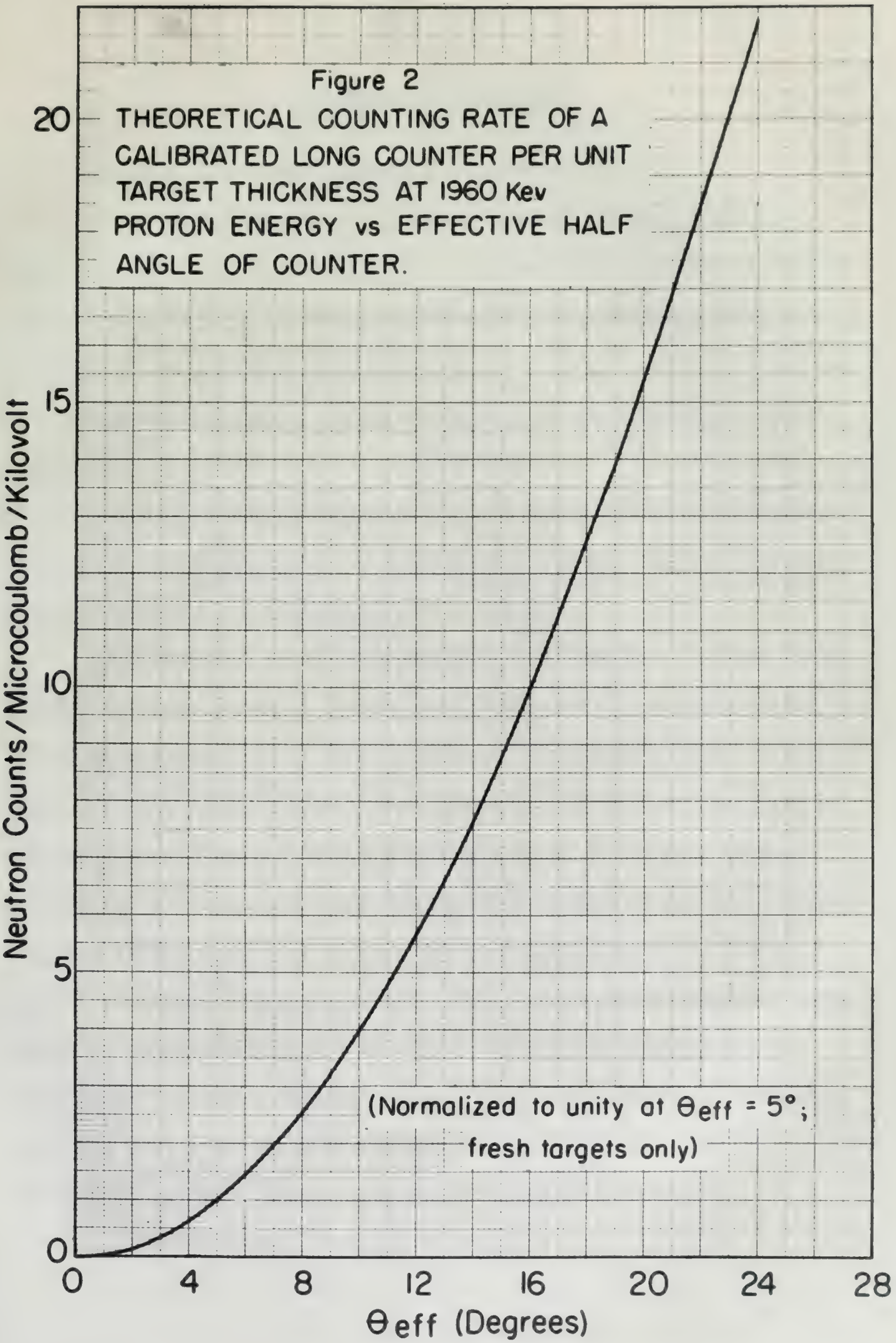

Figure 2

THEORETICAL COUNTING RATE OF A CALIBRATED LONG COUNTER PER UNIT TARGET THICKNESS AT 1960 Kev PROTON ENERGY vs EFFECTIVE HALF ANGLE OF COUNTER.

IX. THE EXPERIMENT AND RESULTS

The purpose of the experiment was:

1. To determine the effective half-angle of the long counter used in this laboratory (7.5-inch paraffin diameter completely shielded with cadmium to reduce background of thermal neutrons) as a function of the distance from the target. With this counter there may be a slight dependence on target thickness; it was desired to check this point.

2. To apply equation (14) to experimental yield curves of targets of several known thicknesses for various counter positions in order to check the validity of this equation.

A convenient method of determining the effective half-angle of the counter for various positions is as follows: Adjust the values of target thickness and counter half-angle to obtain a best fit between the theoretical yield curve[3] (equations 12 and 13 apply) and the experimental curve for one relatively large half-angle of the counter. A calibrated counter placed successively at various distances from the target will give a set of relative counting rates per unit target thickness. These relative counting rates, in conjunction with Figure 2, determine a family of possible curves of effective half-angle versus distance from the target. The correct curve is selected from this family by using the value of θ_{eff} found in fitting the theoretical and experimental curves, as mentioned above.

Three lithium targets of various thicknesses were prepared by evaporating the metal in vacuum onto a tantalum backing rotating eccentrically with the beam axis. This apparatus is mounted on the beam exit tube of the Rockefeller generator, making it unnecessary to expose the target to the atmosphere at any time. The need for fresh targets in correlating target thickness by the "rise" method and by calibrated counter is discussed in Section VIII.

An experimental yield curve was determined for each target and for each of the following distances from counter to the target: 39.4, 18, 11, and 7.5 inches. (The 11- and 18-inch yield curves were omitted on the third target because of lack of time.)

The frequency meter normally used for selecting the desired proton energy was inoperative on the day allotted to this experiment. The standby frequency meter, which was used, had an indeterminable frequency drift that caused the proton energy to be in error by a varying amount up to 3 kev maximum. Because of this, the yield curves from two of the three targets were completely unreliable from the viewpoint of this experiment. The remaining target gave reasonably smooth curves, but they are not considered to be accurate enough for determining the effective half-angle by fitting a theoretical curve. The yields obtained are tabulated in Tables I (A-D) and the experimental curves are presented as Figures 3, 4, 5, and 6. In the regions of interest, enough counts were taken so that the standard deviation could be neglected.

A regulated high-voltage supply was the source of the 2250 volts applied to the BF_3 detector. (This voltage corresponds to the center of the plateau for that particular counter.) The counting rate with a Ra-Be standard source on top of the counter was determined at intervals over a period of three days and never varied more than 2.6 percent.

The BF_3 detector was a Model 3 4CE Mark 2, manufactured by Radiation Counter Laboratories. The output pulses were fed through a preamplifier to a Model 100 amplifier, thence to a Model 1060 multiscaler manufactured by the Atomic Instrument Company. The discriminator is an integral part of the complete multiscaler unit.

Counts were taken for an integral number of microcoulombs of charge on the target. If the beam current changed appreciably during a run, the count was repeated.

Background was small enough to be neglected throughout this experiment.

In an attempt to derive from this experiment some information that would be of immediate use to this laboratory, it was decided to proceed with the assumption that equation (14) is valid and to select that particular curve from the family of possible curves of effective half-angle versus distance from the target which would produce the observed shift in peak position at the various counter positions.

Since the yield is slow varying in the vicinity of 1960-kev proton energy, the counting rates are hardly affected by the frequency drift experienced and may be used for all three targets. In Table VIII, it is shown that the counting rate per unit target thickness is independent of target thickness for the counter half-angles used. An average value of counting rate per unit target thickness for the three targets is calculated, and the relative counting rate determined.

TABLE I (A)

Experimental Data
Counter at 0°, 39.4 inches from Target

Target	Frequency (Megacycles)	Counts	μCoulombs
No. 2	10.468	48	40
	.470	507	40
	.471	2438	40
	.473	5566	40
	.476	7487	40
	.479	8923	40
	.482	10004	40
	.485	10967	40
	.487	22508	80
	.489	22428	80
	.491	21181	80
	.495	19523	80
	.500	8349	40
	.680	9382	160
No. 1	10.680	6431	80
No. 3	10.680	24297	80

TABLE I(B)

Experimental Data
Counter at 0°, 18 inches from Target

Target	Frequency (Megacycles)	Counts	μCoulombs
No. 2	10.478	206	40
	.481	4017	40
	.482	9937	40
	.484	20669	40
	.486	26345	40
	.488	33213	40
	.490	39450	40
	.492	41834	40
	.494	43471	40
	.496	44300	40
	.498	45990	40
	.500	45287	40
	.502	44162	40
	.510	34790	40
	.680	17534	80
No. 1	10.680	25320	80
No. 3	10.680	-	-

TABLE I (C)

Experimental Data
Counter at 0^o, 11 inches from Target

Target	Frequency (Megacycles)	Counts	μCoulombs
No. 2	10.478	586	20
	.480	3864	20
	.483	14506	20
	.485	22813	20
	.489	36572	20
	.493	44621	20
	.496	48686	20
	.498	53171	20
	.500	52869	20
	.502	52078	20
	.506	48899	20
	.680	40968	80
No. 1	10.680	64856	80
No. 3	10.680	-	-

TABLE I (D)

Experimental Data
Counter at 0°, 7.5 inches from Target

Target	Frequency (Megacycles)	Counts	μCoulombs
No. 2	10.4855	2644	20
	.488	14370	20
	.491	29869	20
	.494	47787	20
	.497	62822	20
	.499	68224	20
	.501	72367	20
	.503	81286	20
	.505	86557	20
	.507	85522	20
	.509	84755	20
	.511	82615	20
	.515	73769	20
	.680	33912	40
No. 1	10.680	49807	40
No. 3	10.680	43949	10

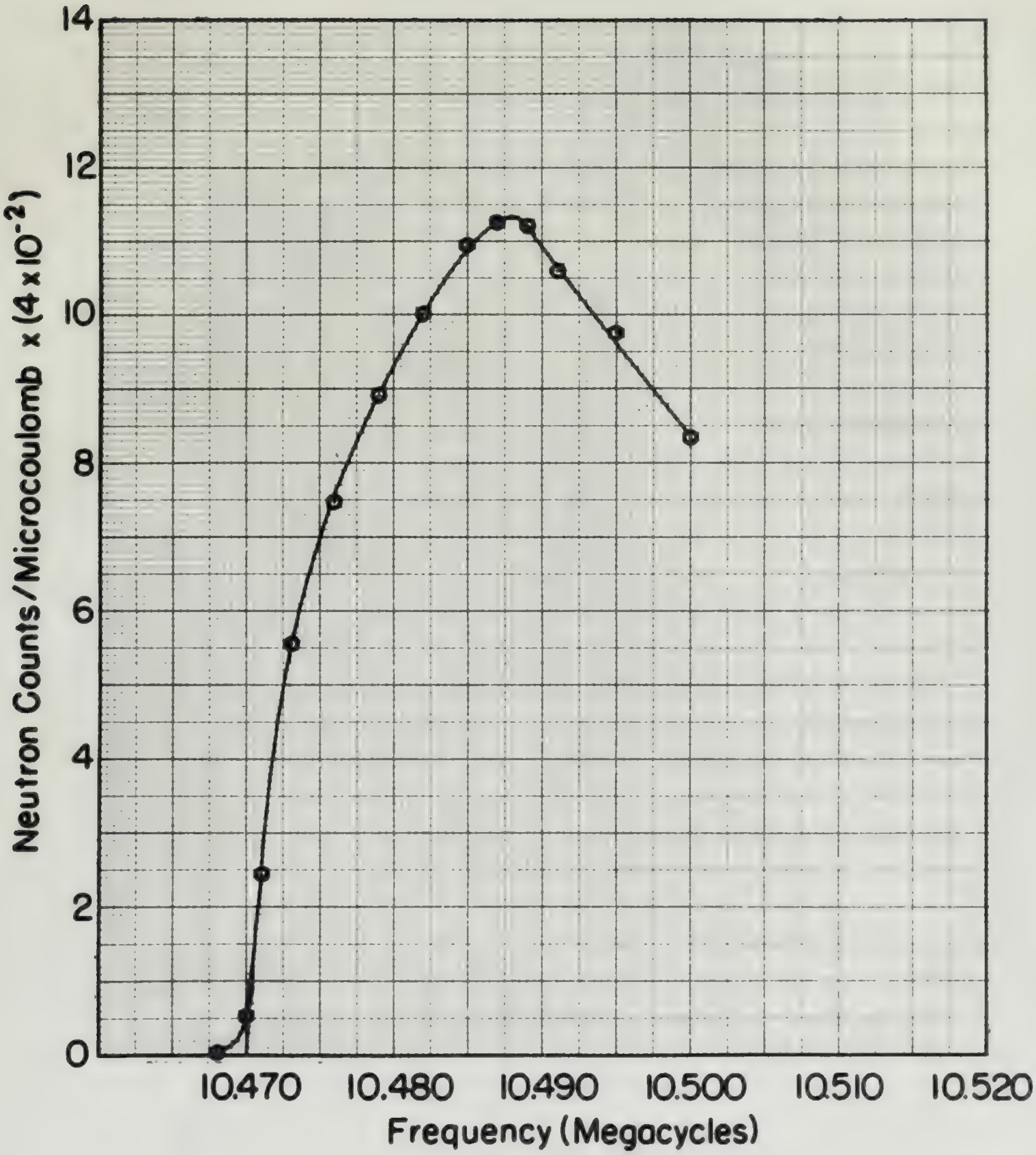

Figure 3

Neutron Yield from Li^7 (p,n) Be^7
Target Thickness 6.44 Kev
Distance from Target to Counter = 39.4 inches

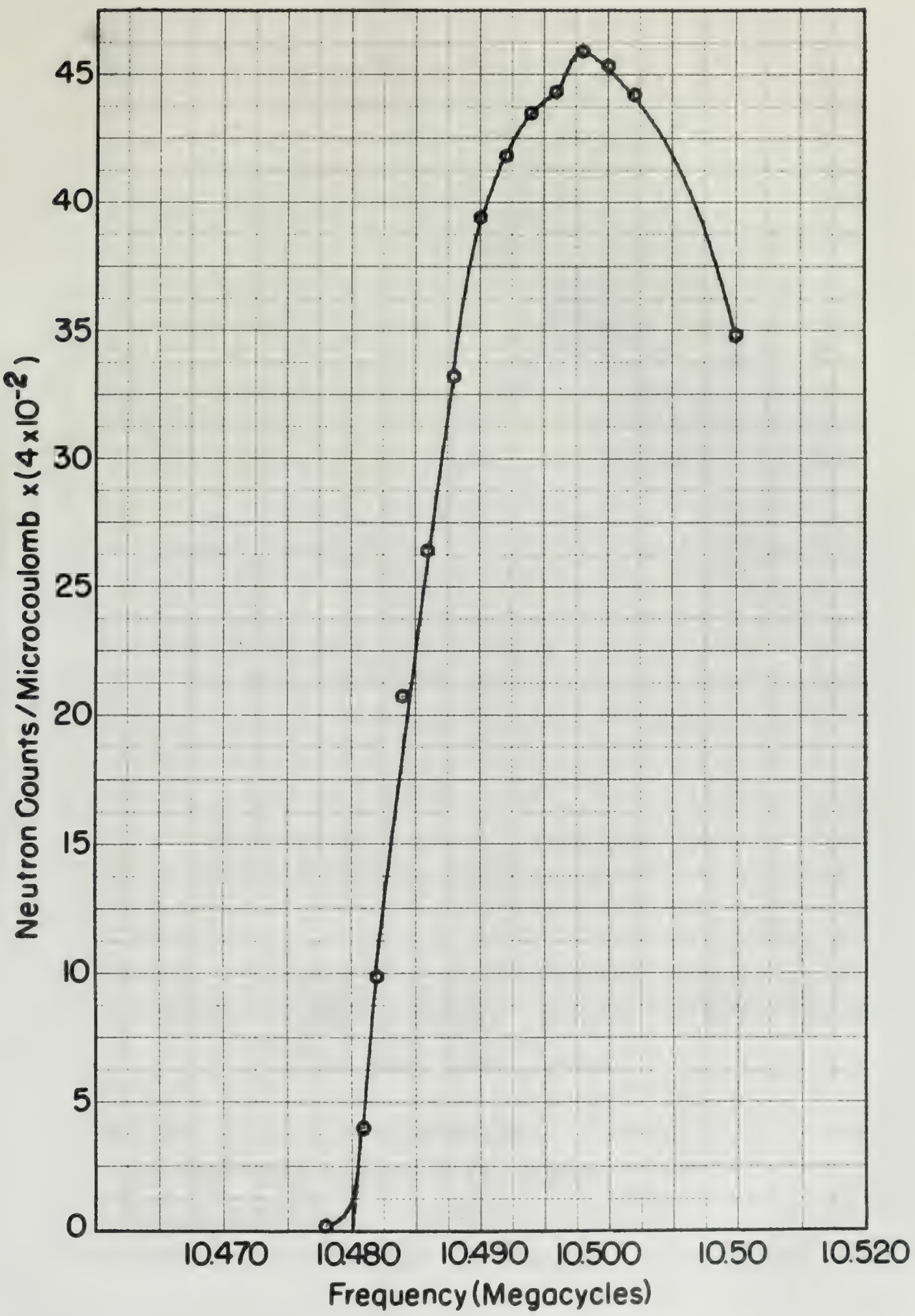

Figure 4

Neutron Yield from Li^7 (p,n) Be^7

Target Thickness 6.44 Kev

Distance from Target to Counter = 18.0 inches

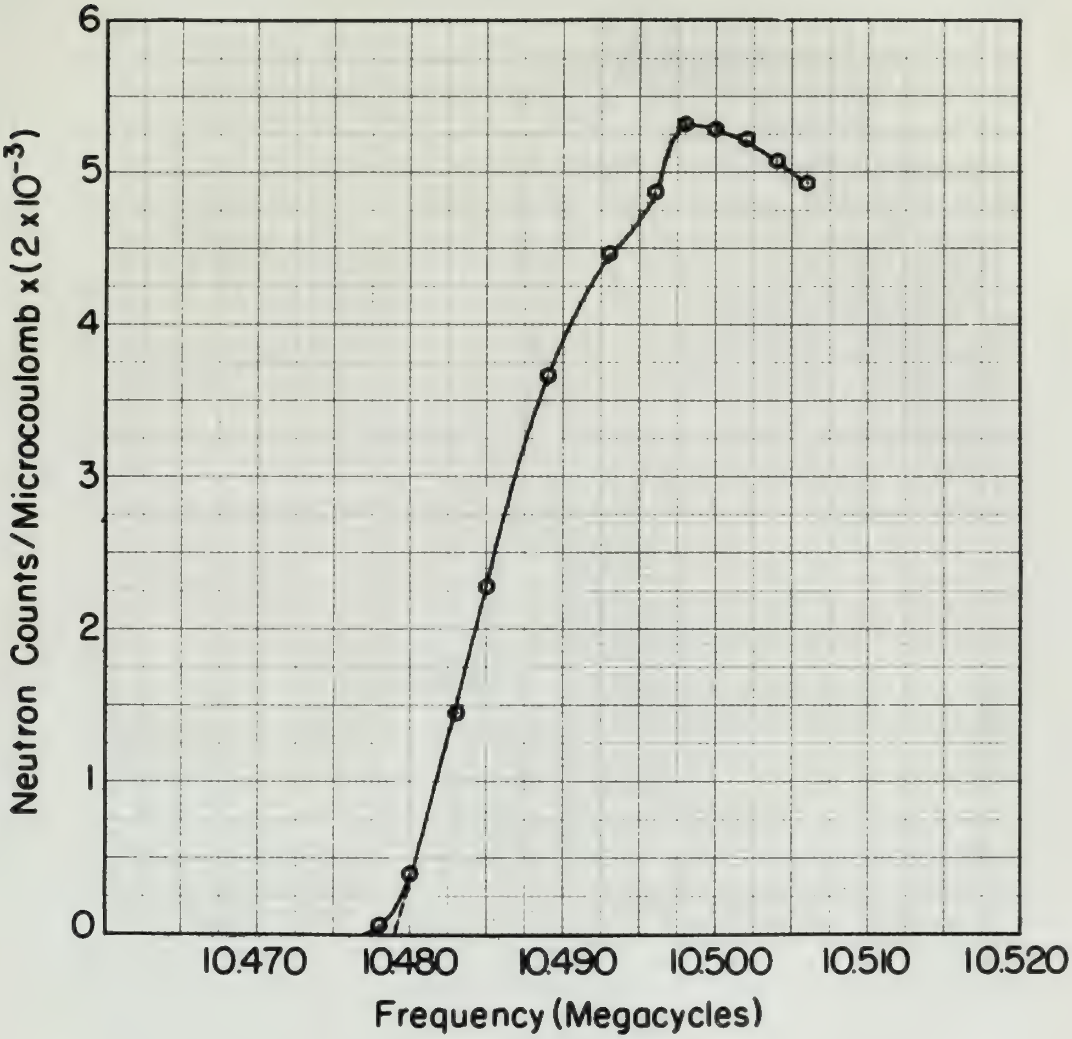

Figure 5

Neutron Yield from Li^7 (p,n) Be^7
Target Thickness 6.44 Kev
Distance from Target to Counter = 11.0 inches

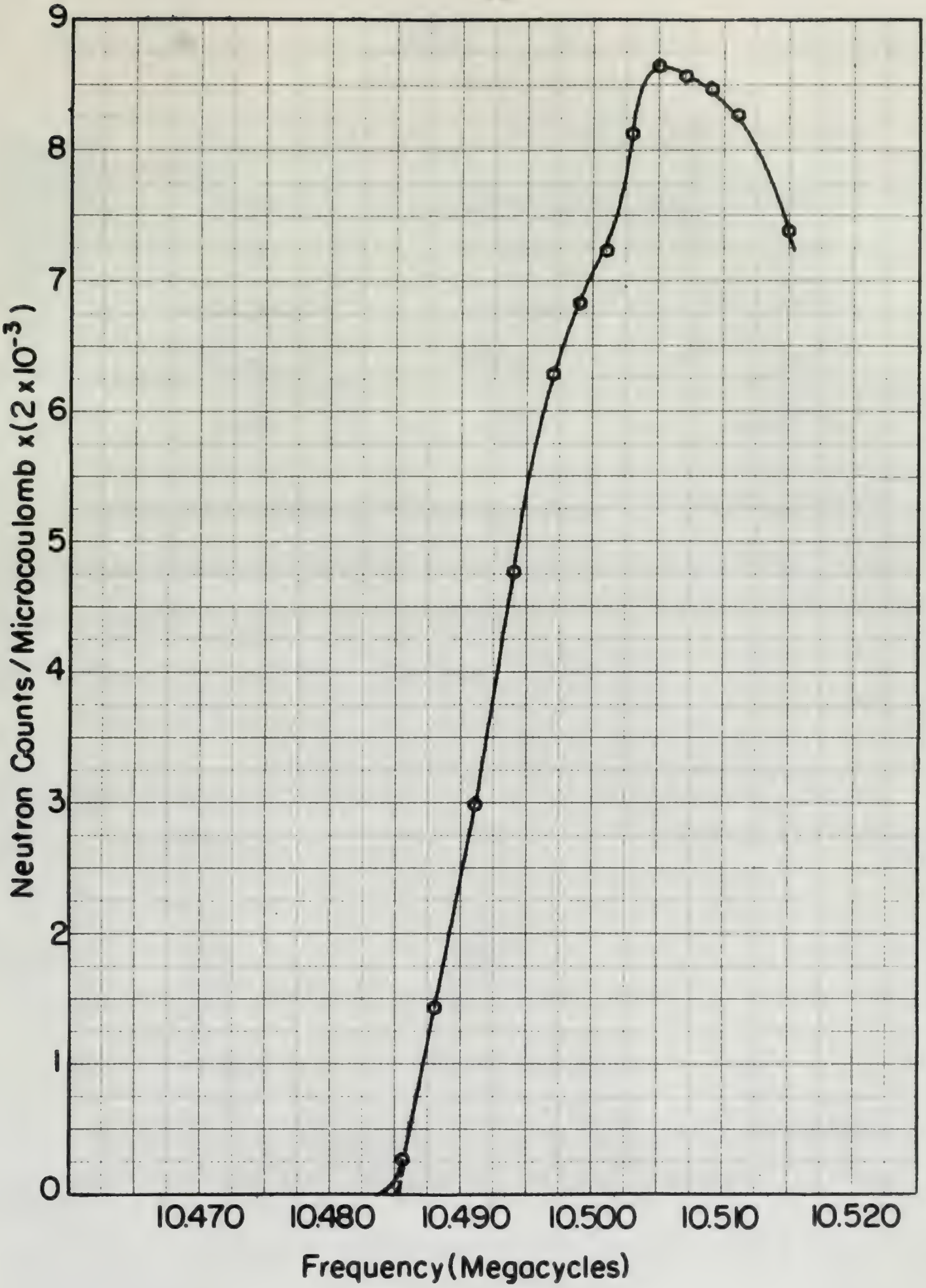

Figure 6

Neutron Yield from Li^7 (p,n) Be^7
Target Thickness 6.44 Kev
Distance from Target to Counter = 7.5 inches

Distance from Target	Counts per 80 μCoulombs at 1953-kev Proton Energy		
	Target 1	Target 2	Target 3
39.4"	6431	4691	24297
18.0	25320	17534	-
11.0	64856	40968	-
7.5	99614	67824	351592

Since the counting rate per unit target thickness should be constant at any given distance from the target, the number unity is arbitrarily assigned to the values obtaining at 39.4 inches and the ratios calculated with reference to it.

Distance from Target	Relative Counting Rates per Unit Target Thickness			
	Target 1	Target 2	Target 3	Average
39.4"	1	1	1	1
18.0	3.94	3.74	-	3.84
11.0	10.08	8.73	-	9.41
7.5	15.49	14.46	14.47	14.81

These average relative counting rates are maintained but are normalized to fit the curve of Figure 2 so that the effective half-angle has in succession the values 3°, 4°, and 5° at 39.4 inches from the target.

Counter Distance	Aver. Ratios	Ratio	θ^{o}_{eff}	Ratio	θ^{o}_{eff}	Ratio	θ^{o}_{eff}
39.4"	1	.361	3.0	.63	4.0	1	5
18.0	3.84	1.386	5.8	2.42	7.7	3.84	9.8
11.0	9.41	3.397	9.2	5.93	12.2	9.41	15.5
7.5	14.81	5.346	11.6	9.33	15.4	14.81	19.6

From these values are drawn the three curves of the family of curves of effective half-angle versus distance from the target (Figure 7).

The difference between the peak and threshold positions in kilocycles is taken directly from the yield curves. These frequency differences (ΔF) are converted into proton energy differences by the relation:

$$(31) \qquad (E_p - E_T) \text{ kev } = \frac{\delta E}{\delta F} \Delta F$$

where $\delta E/\delta F = 0.3575$ kev/kc. for ΔF in kilocycles and a proton energy of 1982 kev. Target thickness is taken as the value of the proton energy difference between the peak and threshold $(E_p - E_T)$ with the counter at 39.4 inches in accordance with equation (14), since the correction term (K) is negligible in this case. Entering Figure 1 with the value of target thickness ($\Delta E = 6.44$ kev), one obtains a value of θ_{eff} for each value of $E_p - E_T$. The results follow:

Distance from Target	ΔF(kc)	$E_p - E_T$	θ_{eff}
39.4"	18	6.44 = ΔE	-
18.0	18	6.44	-
11.0	19	6.80	14°
7.5	20	7.15	18°

The values, θ_{eff} = 14°, 18° are plotted on the family of curves in Figure 7. The most probable curve is now drawn through these two points, giving the best value of the effective half-angle of this particular counter for any counter position between 7.5 and 39.4 inches. This curve may be extrapolated to some extent in either direction.

The following table may be of assistance in applying the above results to a long counter with paraffin diameter slightly different from the 7.5-inch diameter used in this laboratory.

Distance (d)	Tan θ = 3.75/d	θ (Actual)	θ_{eff}
39.4"	.09525	5.43°	4.6°
18.0	.20833	11.77°	9.0°
11.0	.34091	18.82°	14.0°
7.5	.50000	26.57°	18.0°

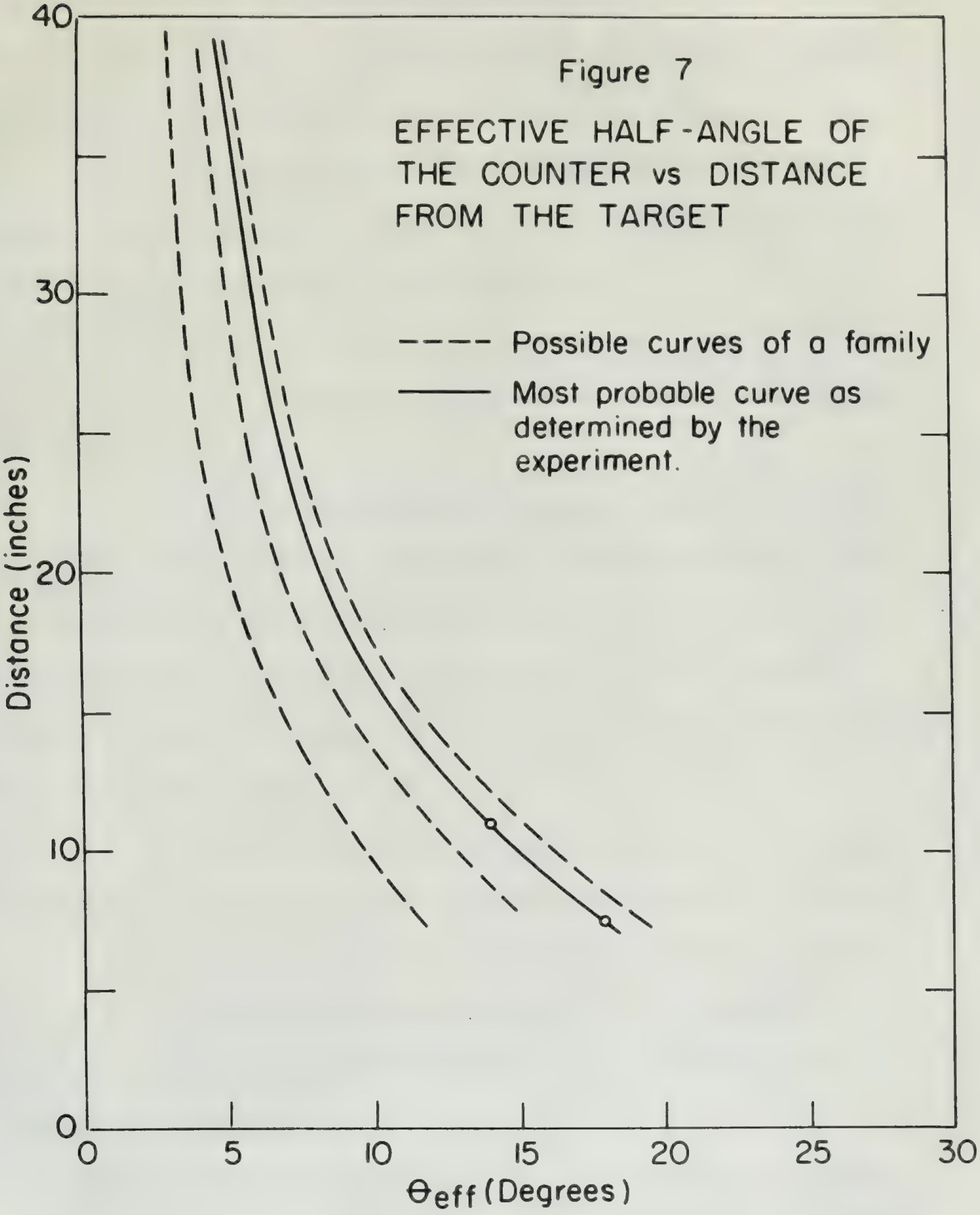
Figure 7
EFFECTIVE HALF-ANGLE OF THE COUNTER vs DISTANCE FROM THE TARGET
---- Possible curves of a family
—— Most probable curve as determined by the experiment.
Distance (inches)
θ_{eff} (Degrees)
0
10
20
30
40
0
5
10
15
20
25
30

X. APPLICATION OF EQUATION (14)

The determination of target thickness, as given by equation (14), consists of four steps:

A. Determination of the effective half-angle of the counter. This value may be taken directly from Figure 7 when using the long counter employed in this laboratory.

B. Determination of the reaction threshold by either

1. Extrapolating the lower linear portion of the curve to the axis; or

2. A supplementary experiment using a target of about 20-kev thickness and an effective half-angle of about 4 degrees after the method described in Section VII. This method is useful only if the proton energy is very closely controlled and measured so that measurements of the threshold value may be duplicated within very narrow limits.

C. Measurement of the energy difference between peak and threshold ($E_p - E_T$) directly from the experimental yield curve.

D. Enter Figure 1 with the appropriate values of θ_{eff} and $E_p - E_T$ to get target thickness directly. For endoergic reactions other than the $Li(p,n)Be^7$ reaction, target thickness must be calculated by equation (14).

One may also use Figures 1 and 7 for selecting a suitable counter position, assuming that a rough estimate of target thickness is available, either from past measurements of thickness or by visual

inspection. In this connection, the lower dashed portions of the curves in Figure 1 should be avoided, as the peak position is not very sensitive to target thickness in these regions.

XI. CONCLUSIONS AND RECOMMENDATIONS

As a result of this study, it is concluded that the most accurate value of target thickness will be obtained by fitting a theoretical yield curve to the experimentally determined curve as described by Bonner and Butler[3] and discussed herein. However, the method described in this thesis should give very good approximations of target thickness with but little effort from the very manner in which the effective half-angle of the counter has been assigned. The ability to measure the target thickness by the rise method for various counter positions is certainly an advantage as higher counting rates can be obtained with the use of a lower beam current; hence, the effects of ageing of the target while measuring the thickness will be decreased. This could be important when using thin targets, as they are subject to considerable thickening after only a few hours of use (Hinchey, Preston, and Stilson, unpublished data).

The information presented in Section VII dealing with proton energy resolution leads to the conclusion that this method cannot be expected to give nearly so good results for thicknesses of less than two kilovolts as would be expected for the range from two to twenty kilovolts.

To extend the results presented in this thesis, the following recommendations are made:

A. Perform the experiment outlined in Section IX in order to:

1. Obtain a more accurate value of effective counter half-angle if possible.

2. Determine whether the effective half-angle varies with target thickness. Any such dependence should be small and could be presented as a family of curves similar to the curve of effective half-angle versus distance of the counter from the target (Figure 1).

3. Check the accuracy of the results presented herein for various counter positions and target thicknesses.

B. Perform a series of experiments to determine the difference between the actual threshold and the apparent threshold as determined by a linear extrapolation to the axis. This information would be particularly helpful when using very thin targets (less than 2 kev).

C. Determine the optimum dimensions and properties of a counter to be used specifically for measuring target thickness. In this connection, consider the fact that the counter will be used for endoergic reactions other than the $Li^7(p,n)Be^7$ reaction.

D. Make calculations for the $T^3(p,n)He^3$ reaction similar to those presented here for the $Li^7(p,n)Be^7$ reaction, inasmuch as tritium targets are commonly used in this laboratory as a neutron source.

APPENDIX A

DERIVATION OF G

In deriving the expressions for the fraction G of neutrons from an elemental thickness of target which enters the counter, Figure 8 applies throughout. The basic assumption is that the neutrons are emitted isotropically in the center-of-mass system. Sphere A represents the locus of neutron velocity vectors (V_n) in the center-of-mass system. The velocity of the center of mass (V_{cm})is then added to each point of sphere A to obtain sphere B which is then the locus of neutron velocity vectors in the laboratory system. The counter subtends a solid angle at the target in the form of a cone, the half-angle (half of the apex angle) of which is designated by θ. If sphere B lies entirely within this cone, then all of the neutrons will strike the counter. If the velocity of the center of mass is less than the neutron velocity in the center-of-mass system, then neutrons from an area A_H on the sphere B will strike the counter. For the situation intermediate between these two, there will be a high-energy group of neutrons from area A_H and a lower-energy group from area A_L intercepted by the counter. The number of neutrons in the groups has the same ratio to the total number of neutrons as the area in question bears to the total area of the sphere.

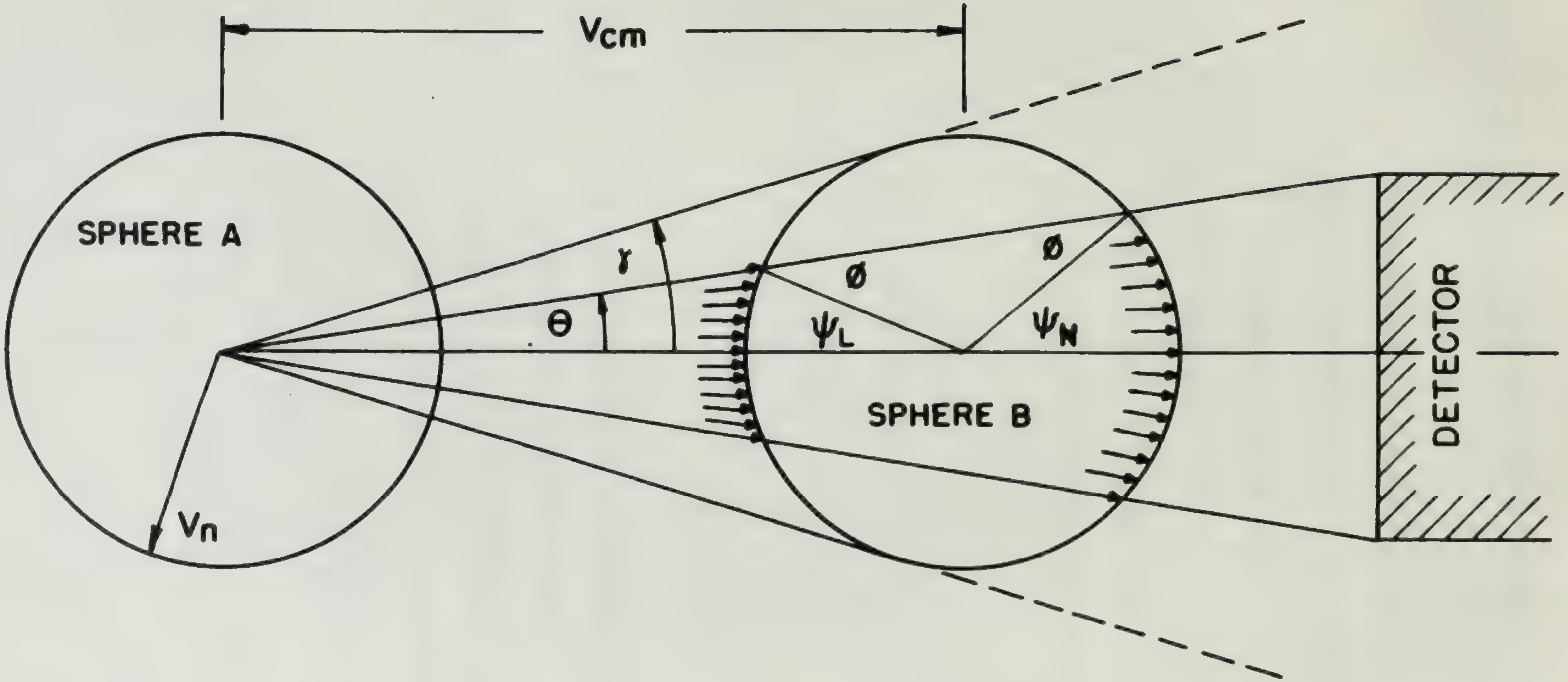

Figure 8

SCHEMATIC REPRESENTATION OF THE MECHANICS OF AN ENDOERGIC REACTION JUST ABOVE THRESHOLD

The following summary is given to clarify the three situations:

E = proton energy (instantaneous)

E_o = proton energy (incident upon the target)

E_T = proton energy (threshold)

E_c = proton energy ($\gamma = \theta$)

E_L = proton energy ($\gamma = \pi/2$; $V_n = V_{cm}$)

G = fraction of neutrons entering the counter.

G	E	γ	Remarks
G_1	$E_T < E < E_c$	$\gamma < \theta$	All neutrons strike counter
G_2	$E_c < E < E_L$	$\theta < \gamma < \pi/2$	Two groups
G_3	$E_L < E$	$\gamma = \pi$	One group

V_n = neutron velocity in center-of-mass system

V_{cm} = velocity of center of mass

$A_{H,L}$ = area on surface of sphere B through which pass the high- and low-energy groups of neutrons respectively, which are intercepted by the counter.

$$\frac{V_{cm}}{\sin(\pi - \phi)} = \frac{V_n}{\sin\theta} \qquad \text{or} \qquad \frac{V_{cm}}{\sin\phi} = \frac{V_n}{\sin\theta}$$

Therefore $\sin\phi = \frac{V_{cm}}{V_n}\sin\theta$

$$\cos\phi = \left[1 - \left(\frac{V_{cm}}{V_n}\right)^2 \sin^2\theta\right]^{1/2}$$

Area: $A_{H,L} = 2\pi V_n^2 (1 - \cos\Psi_{H,L})$

$$\cos\Psi_H = \cos(\phi + \theta) = \cos\phi\cos\theta - \sin\phi\sin\theta$$

$$= \cos\theta\left[1 - \left(\frac{V_{cm}}{V_n}\right)^2 \sin^2\theta\right]^{1/2} - \frac{V_{cm}}{V_n}\sin^2\theta$$

$$\cos\Psi_L = \cos(\phi - \theta) = \cos\phi\cos\theta + \sin\phi\sin\theta$$

$$= \cos\theta\left[1 - \left(\frac{V_{cm}}{V_n}\right)^2 \sin^2\theta\right]^{1/2} + \frac{V_{cm}}{V_n}\sin^2\theta$$

$$G = \frac{A_H + \delta A_L}{A_{sphere}} \quad \text{where} \quad \begin{cases} \delta = 1 \text{ for } V_{cm} > V_n \\ \delta = 0 \text{ for } V_{cm} < V_n \end{cases}$$

Therefore

$$G = 1/2 \left\{ 1 - \cos\theta \left[1 - \left(\frac{V_{cm}}{V_n}\right)^2 \sin^2\theta \right]^{1/2} + \frac{V_{cm}}{V_n} \sin^2\theta \right\}$$

$$+ 1/2 \quad \delta \left\{ 1 - \cos\theta \left[1 - \left(\frac{V_{cm}}{V_n}\right)^2 \sin^2\theta \right]^{1/2} - \frac{V_{cm}}{V_n} \sin^2\theta \right\}$$

$$(32a) \quad G = G_1 = 1 \quad . \; . \; . \; . \; . \; . \; . \; . \; . \; . \; . \; . \quad \text{for } E < E_c$$

$$(32b) \quad G = G_2 = 1 - \cos\theta \left[1 - \left(\frac{V_{cm}}{V_n}\right)^2 \sin^2\theta \right]^{1/2} \text{for } E_c < E < E_L$$

$$(32c) \quad G = G_3 = 1/2 \left\{ 1 - \cos\theta \left[1 - \left(\frac{V_{cm}}{V_n}\right)^2 \sin^2\theta \right]^{1/2} + \frac{V_{cm}}{V_n} \sin^2\theta \right\} . \; . \; . \; . \; . \quad \text{for } E > E_L$$

When $V_n = V_{cm}$, $G_2 = G_3 = \sin^2\theta$.

Let m_1 = projectile particle mass

m_2 = target particle mass

m_3 = resultant particle mass

m_4 = product nucleus mass

Q = Q-value of reaction (negative for endoergic reactions)

V_1 = projectile particle velocity in laboratory system.

(33) $$V_{cm} = \frac{m_1}{m_1 + m_2} V_1 = \frac{(2m_1E)^{1/2}}{m_1 + m_2}$$

(34) $$V_n = \left\{ \frac{2m_2 m_4}{m_3(m_1 + m_2)^2} \left[E + \frac{(m_1 + m_2)}{m_2} Q \right] \right\}^{1/2} \text{(reference 1)}$$

But $\frac{m_1 + m_2}{m_2} Q = - E_T$

(35) $$V_n = \left\{ \frac{2m_2 m_4}{m_3(m_1 + m_2)^2} \left(E - E_T \right) \right\}^{1/2} = \text{const } (E - E_T)^{1/2}$$

$$\left(\frac{V_{cm}}{V_n}\right)^2 = \frac{m_1 m_3}{m_2 m_4} \left(\frac{E}{E - E_T}\right)$$

Hence, the expressions for $G_{1,2,3}$ may be written:

(36a) $G_1 = 1$ . . . . $E < E_c$

(36b) $G_2 = 1 - \cos\theta \left[1 - \frac{m_1 m_3}{m_2 m_4} \frac{E \sin^2\theta}{(E - E_T)} \right]^{1/2}$. $E_c < E < E_L$

(36c) $$G_3 = 1/2 \left\{ 1 - \cos\theta \left[1 - \frac{m_1 m_3}{m_2 m_4} \frac{E \sin^2\theta}{(E - E_T)} \right]^{1/2} + \sin^2\theta \left[\frac{m_1 m_3}{m_2 m_4} \frac{E}{(E - E_T)} \right]^{1/2} \right\}$$ . . . . . $E > E_L$

If E_c is defined as the proton energy at which the solid angle of the neutron cone is equal to the solid angle subtended at the target by the counter (i.e., $\gamma = \theta$ at $E = E_c$), then:

$$\sin \theta = \frac{V_n}{V_{cm}}$$

$$\sin^2 \theta = \left(\frac{V_n}{V_{cm}}\right)^2 = \frac{m_2 m_4}{m_1 m_3} \left(\frac{E_c - E_T}{E_c}\right)$$

$$E_c = \frac{E_T}{1 - \frac{m_1 m_3}{m_2 m_4} \sin^2 \theta} \tag{37}$$

E_c values are calculated for various θ (for the Li(p,n) reaction only) in Table II, Appendix B, and presented as a curve in Figure 9.

(38) Let $k = \left(1 - \frac{m_1 m_3}{m_2 m_4} \sin^2 \theta\right)^{1/2} \cos \theta = \left(\frac{E_T}{E_c}\right)^{1/2} \cos \theta$

(39) and $b = \left(\frac{m_1 m_3}{m_2 m_4}\right)^{1/2} \sin^2 \theta$

The equations for $G_{1,2,3}$ become:

(40a) $G_1 = 1$ . . . . $E < E_c$

(40b) $G_2 = 1 - k(\frac{E - E_c}{E - E_T})^{1/2}$ . . . . $E_c < E < E_L$

(40c) $G_3 = 1/2 \left[1 - k(\frac{E - E_c}{E - E_T})^{1/2} + b(\frac{E}{E - E_T})^{1/2} \right]$. $E > E_L$

where E_L is given by evaluating E_c at $\theta = \pi/2$ in equation (37) above:

(41) $$E_L = \frac{E_T}{1 - \frac{m_1 m_3}{m_2 m_4}}$$

APPENDIX B

COMPUTATIONS RELATIVE TO THE $Li^7(p,n)Be^7$ REACTION

The following values will be used in connection with the $Li^7(p,n)Be^7$ reaction:

$E_T = 1.882$ Mev

$Q = -1.6456$ Mev

$m_1 = m(p) = 1.007593$

$m_2 = m(Li^7) = 7.01659$

$m_3 = m(n) = 1.008982$

$m_4 = m(Be^7) = 7.01697$

The threshold and Q-values are those determined by Herb, Snowden, and Sala[12], while the nuclear mass values are from a compilation used in this laboratory (from numerous sources).

$m_1 + m_2 = 8.024183$

$m_1 m_3 = 1.016632$

$m_2 m_4 = 49.235202$

$$\frac{m_1 m_3}{m_2 m_4} = 0.020687$$

$$1 - \frac{m_1 m_3}{m_2 m_4} = 0.9793513$$

$$(42) \qquad E_L = \frac{E_T}{1 - \frac{m_1 m_3}{m_2 m_4}} = 1921.68 \text{ kev} = E_T + 39.68 \text{ kev.}$$

$$(43) \qquad E_c = \frac{E_T}{1 - \frac{m_1 m_3}{m_2 m_4} \sin^2 \theta} = \frac{1882}{1 - 0.0206487 \sin^2 \theta} \text{ kev.}$$

Equation (43) is used for computing E_c (Table II) for effective half-angles of the counter up to 30 degrees, and the results are given as the curve of Figure 9.

Values of k for various half-angles of the counter are calculated from the relation (equation 38):

$$k = \left(1 - \frac{m_1 m_3}{m_2 m_4} \sin^2 \theta\right)^{1/2} \cos \theta = \left(\frac{E_T}{E_c}\right)^{1/2} \cos \theta.$$

These k values are given in Table III for later use in other computations.

In Table IV is the computed value of

$$\frac{4(E_c - E_T)}{k^2 + 1/k^2 - 2}$$

used in Section VI for determining the region of the geometric peak.

Tables V (A-G) includes the calculations for the correction term K and target thickness ΔE for various values of the proton energy difference between the geometric peak and threshold $(E_p - E_T)$ according to equation (14):

$$\Delta E = E_p - E_T - K \qquad (14)$$

where $K = \left[(E_p - E_T)^{1/2} - k(E_p - E_c)^{1/2} \right]^2$

Curves of ΔE versus $(E_p - E_T)$ for values of Θ_{eff} from 4 to 28 degrees are constructed from the results of Table V and presented as Figure 1.

TABLE II

Evaluation of E_c for various effective half-angles of the counter
(Equations 37 and 43)

θ	$\sin^2\theta$	$.0206487\ \sin^2\theta$	E_T/E_c	E_c (kev)
2	.001218	.000025	.999975	1882.047
3	.002739	.000057	.999943	1882.107
4	.004866	.000100	.999900	1882.188
5	.007597	.000157	.999843	1882.295
6	.010927	.000226	.999774	1882.425
7	.014852	.000307	.999693	1882.577
8	.019368	.000400	.999600	1882.753
9	.024470	.000505	.999495	1882.950
10	.030154	.000623	.999377	1883.173
11	.036408	.000752	.999248	1883.416
12	.043227	.000893	.999107	1883.682
13	.050603	.001045	.998955	1883.968
14	.05853	.001209	.998791	1884.278
16	.07598	.001569	.998431	1884.957
18	.09549	.001972	.998028	1885.718
20	.11698	.002415	.997585	1886.556
22	.14033	.002898	.997102	1887.469
24	.16544	.003416	.996584	1888.450
26	.19217	.003968	.996032	1889.497
28	.22040	.004551	.995449	1890.604
30	.25000	.005162	.994838	1891.765

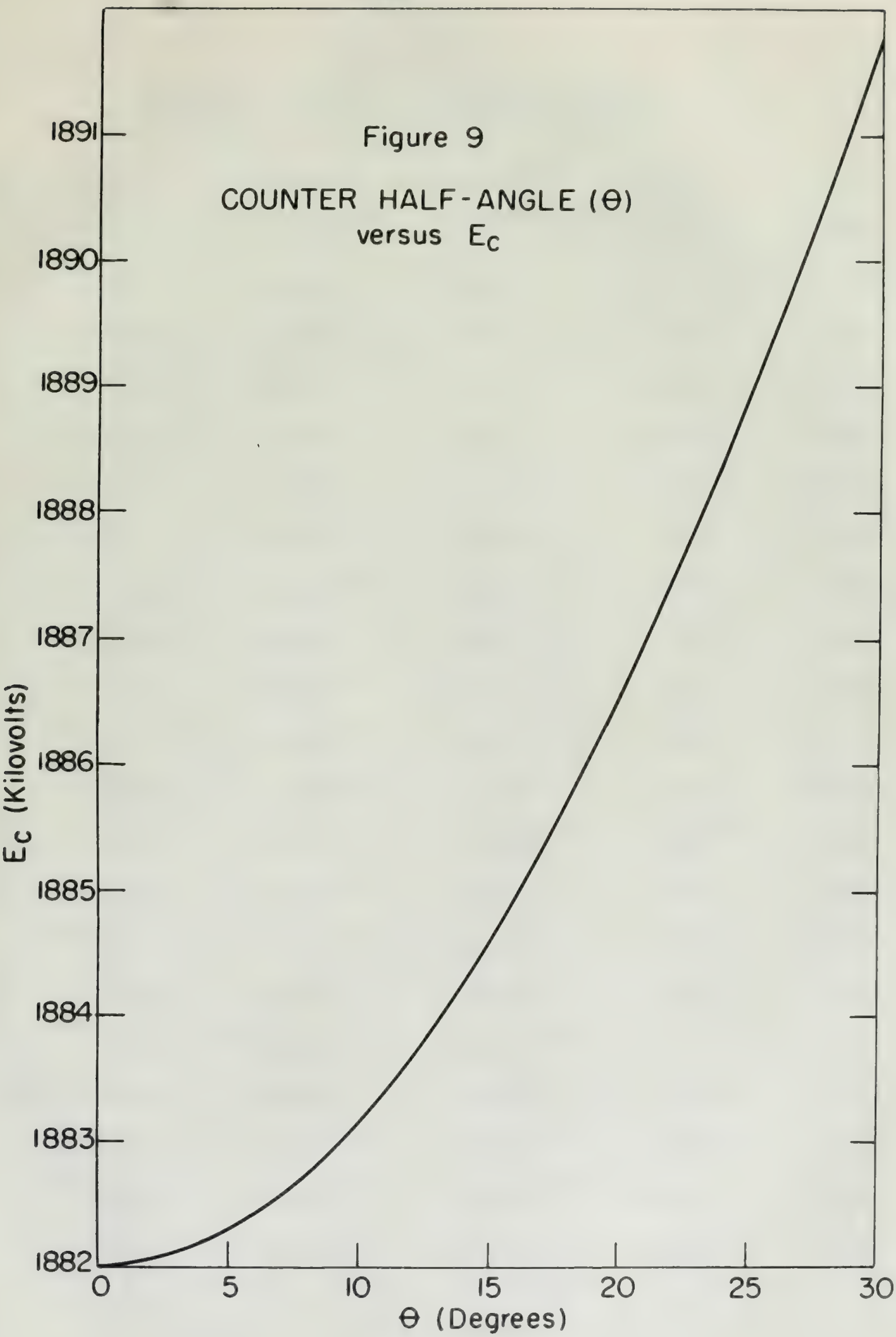

Figure 9

COUNTER HALF-ANGLE (θ) versus E_c

TABLE III

Evaluation of k as given by Equation (38)

θ°	E_c-E_T	(E_T/E_c)	$(E_T/E_c)^{1/2}$	cos θ	k
2	.047	.99998	.99999	.99939	.99938
3	.107	.99994	.99997	.99863	.99860
4	.188	.99990	.99995	.99756	.99751
5	.295	.99984	.99992	.99619	.99611
6	.425	.99977	.99988	.99452	.99441
7	.577	.99969	.99984	.99255	.99239
8	.753	.99960	.99980	.99027	.99007
9	.950	.99950	.99975	.98769	.98744
10	1.173	.99938	.99969	.98481	.98450
11	1.416	.99925	.99962	.98163	.98126
12	1.682	.99911	.99955	.97815	.97771
13	1.968	.99896	.99948	.97437	.97386
14	2.278	.99879	.99940	.97030	.96972
16	2.957	.99843	.99921	.96126	.96050
18	3.718	.99803	.99901	.95106	.95012
20	4.556	.99759	.99879	.93969	.93855
22	5.469	.99710	.99855	.92718	.92584
24	6.450	.99658	.99829	.91355	.91199
26	7.497	.99603	.99801	.89879	.89700
28	8.604	.99545	.99772	.88295	.88094
30	9.765	.99484	.99742	.86603	.86380

TABLE IV

Evaluation of $R = 4(E_c-E_T)/(k^2+1/k^2-2)$ (Section VI)

Note: k and $(E_c - E_T)$ are evaluated in Table III

θ	k^2	$1/k^2$	(k^2+1/k^2-2)	$1/4(k^2+1/k^2-2)$	E_c-E_T	R
2	.99876	1.00124	0	0	0.047	∞
3	.99720	1.00281	.00001	.0000025	0.107	42800
4	.99503	1.004995	.000025	.000005	0.188	37600
5	.99224	1.00782	.00006	.000015	0.295	19667
6	.98884	1.01129	.00013	.000033	0.425	12878
7	.98484	1.01539	.00023	.000058	0.577	9948
8	.98024	1.02016	.00040	.000100	0.753	7530
9	.97504	1.02560	.00064	.000160	0.950	5937
10	.96925	1.03173	.00098	.000245	1.173	4788
11	.96287	1.03856	.00143	.000358	1.416	3955
12	.95592	1.04611	.00203	.000508	1.682	3311
13	.94841	1.05440	.00281	.000703	1.968	2799
14	.94033	1.06346	.00379	.000948	2.278	2402
16	.92257	1.08393	.00650	.001625	2.957	1819
18	.90273	1.10775	.01048	.002620	3.718	1419
20	.88089	1.13522	.01611	.004028	4.556	1131
22	.85718	1.16662	.02380	.005950	5.469	919
24	.83172	1.20233	.03405	.008513	6.450	757
26	.80462	1.24282	.04744	.011860	7.497	632
28	.77605	1.28858	.06463	.016158	8.604	532
30	.74613	1.34025	.08638	.021595	9.765	452

TABLE V(A-G)

Evaluation of the correction term K and target thickness ΔE in Equation 14 for an effective counter half-angle θ_{eff} of 4-28 degrees

θ_{eff}	(E_p-E_T)	$(E_p-E_T)^{\frac{1}{2}}$	(E_p-E_c)	$(E_p-E_c)^{\frac{1}{2}}$	$k(E_p-E_c)^{\frac{1}{2}}$	$K^{\frac{1}{2}}$	K	ΔE
4	2	1.41421	1.812	1.34617	1.34282	.07139	.005	2
	4	2.00000	3.812	1.95245	1.94759	.05241	.003	4
	8	2.82843	7.812	2.79500	2.78804	.04039	.002	8
	12	3.46410	11.812	3.43685	3.42829	.03581	.001	12
	16	4.00000	15.812	3.97644	3.96654	.03346	.001	16
	20	4.47214	19.812	4.45108	4.44000	.03214	.001	20
8	2	1.41421	1.247	1.11669	1.10560	.30861	.095	1.9
	4	2.00000	3.247	1.80193	1.78404	.21596	.047	4
	8	2.82843	7.247	2.69204	2.66531	.16312	.027	8
	12	3.46410	11.247	3.35365	3.32035	.14375	.021	12
	16	4.00000	15.247	3.90477	3.86600	.13400	.018	16
	20	4.47214	19.247	4.38712	4.34356	.12858	.017	20
12	2	1.41421	0.318	.56392	.55135	.86286	.745	1.3
	4	2.00000	2.318	1.52249	1.48855	.51145	.262	3.7
	8	2.82843	6.318	2.51355	2.45752	.37091	.138	7.9
	12	3.46410	10.318	3.21216	3.14056	.32354	.105	11.9
	16	4.00000	14.318	3.78388	3.69954	.30046	.090	15.9
	20	4.47214	18.318	4.27999	4.18459	.28755	.083	19.9

TABLE V(A-G)
(Continued)

θ_{eff}	(E_p-E_T)	$(E_p-E_T)^{\frac{1}{2}}$	(E_p-E_c)	$(E_p-E_c)^{\frac{1}{2}}$	$k(E_p-E_c)^{\frac{1}{2}}$	$K^{\frac{1}{2}}$	K	ΔE
16	4	2.00000	1.043	1.02127	0.98093	1.01907	1.039	3.0
	8	2.82843	5.043	2.24569	2.15699	.67144	.451	7.5
	12	3.46410	9.043	3.00717	2.88839	.57571	.331	11.7
	16	4.00000	13.043	3.611514	3.46886	.53114	.282	15.7
	20	4.47214	17.043	4.12832	3.96525	.50689	.257	19.7
20	5	2.23607	0.444	.66633	.62538	1.61069	2.594	2.4
	8	2.82843	3.444	1.85580	1.74176	1.08667	1.181	6.8
	12	3.46410	7.444	2.72836	2.56070	.90340	.816	11.2
	16	4.00000	11.444	3.38289	3.17501	.82499	.681	15.3
	20	4.47214	15.444	3.92984	3.68835	.78379	.614	19.4
24	8	2.82843	1.550	1.24495	1.13538	1.69305	2.867	5.1
	12	3.46410	5.550	2.35584	2.14850	1.31560	1.731	10.3
	16	4.00000	9.550	3.09033	2.81835	1.18165	1.396	14.6
	20	4.47214	13.550	3.68285	3.35872	1.11342	1.240	18.8
28	10	3.16278	1.396	1.18152	1.04085	2.12193	4.503	5.5
	12	3.46410	3.396	1.84282	1.62341	1.84069	3.388	8.6
	16	4.00000	7.396	2.71956	2.39577	1.60423	2.574	13.4
	20	4.47214	11.396	3.37580	2.97388	1.49826	2.245	17.8

TABLE VI (A)

Evaluation of terms included in equation 30

θ	$\cos\theta$	$\sin^2\theta$	$\frac{\cos\theta}{\sin^2\theta}$	$\frac{.0103\cos\theta}{\sin^2\theta}$	$\frac{.71850}{\sin^2\theta}$	$\frac{19.385\cos\theta}{\sin^2\theta}$
3	.99863	.00274	.00274	.00003	.00197	.05311
5	.99619	.00760	.00757	.00008	.00546	.14674
7	.99255	.01485	.01474	.00015	.01099	.28573
10	.98481	.03015	.02969	.00031	.02199	.57554
13	.97437	.05060	.04930	.00051	.03636	.95568
16	.96126	.07598	.07304	.00075	.05459	1.41588
20	.93969	.11698	.10992	.00113	.08405	2.13080
24	.91355	.16543	.15113	.00156	.11886	2.92966

TABLE VI (B)

$\ln 78 = 4.35671$

ΔE (kev)	$\ln(78 - \Delta E)$	$\ln 78 - \ln(78 - \Delta E)$
1	4.34381	.01290
2	4.33073	.02598
4	4.30407	.05264
8	4.24850	.10821
12	4.18965	.16706
16	4.12713	.22958
20	4.06044	.29627
24	3.98898	.36773
28	3.91202	.44469
32	3.82864	.52807

TABLE VI (C)

θ°	$(2/\sigma - Z)N_c$	
3	$.00337\ \Delta E + 0.05311$	$[\ln 78 - \ln(78 - \Delta E)]$
5	$.00935\ \Delta E + 0.14674$	"
7	$.01859\ \Delta E + 0.28573$	"
10	$.03749\ \Delta E + 0.57554$	"
13	$.06250\ \Delta E + 0.95568$	"
16	$.09408\ \Delta E + 1.41588$	"
20	$.14549\ \Delta E + 2.13080$	"
24	$.20687\ \Delta E + 2.92996$	"

Evaluation of terms appearing in equation 30

TABLE VII (A)

Evaluation of equation 30 for a counter half-angle of 3 degrees

ΔE	$.00337\ \Delta E$	$.05311\ \ell n(78/78-\Delta E)$	$(2/\sigma Z)N_c$	$N_c \propto$	$(2/\sigma Z)N_c/\Delta E$
1	.00337	.00069	.00406	1.000	.00406
2	.00674	.00138	.00812	2.000	.00406
4	.01348	.00280	.01628	4.001	.00407
8	.02696	.00575	.03271	8.057	.00409
12	.04044	.00873	.04917	12.111	.00410
16	.05392	.01219	.06611	16.283	.00413
20	.06740	.01573	.08313	20.475	.00416
24	.08088	.01953	.10041	24.732	.00418
28	.09436	.02362	.11798	29.059	.00421
30	.10784	.02805	.13589	33.470	.00425

TABLE VII (B)

Evaluation of equation 30 for a counter half-angle of 5 degrees

ΔE	$.00935\Delta E$	$.1467\ \ln(78/78-\Delta E)$	$(2/\sigma Z)N_c$	$N_c \propto$	$(2/\sigma Z)N_c/\Delta E$
1	.00935	.00189	.01124	1.0000	.01124
2	.01870	.00381	.02251	2.003	.01126
4	.03740	.00772	.04512	4.014	.01128
8	.07480	.01588	.09068	8.068	.01134
12	.11220	.02451	.13671	12.163	.01139
16	.14960	.03369	.18329	16.307	.01146
20	.18700	.04347	.23047	20.504	.01152
24	.22440	.05396	.27836	24.765	.01160
28	.26180	.06525	.32705	29.097	.01168
32	.29920	.07749	.37669	33.513	.01177

TABLE VII (C)

Evaluation of equation 30 for a counter half-angle of 7 degrees

ΔE	$.01859\ \Delta E$	$.28573\ \ln(78/78-\Delta E)$	$(2/\sigma Z)N_c$	$N_c \alpha$	$(2/\sigma Z)N_c/\Delta E$
1	.01859	.00369	.02228	1.0000	.02228
2	.03718	.00742	.04460	2.002	.02230
4	.07436	.01504	.08940	4.013	.02235
8	.14872	.03092	.17964	8.063	.02247
12	.22308	.04773	.27081	12.155	.02257
16	.29744	.06560	.36304	16.294	.02269
20	.37180	.08465	.45645	20.487	.02282
24	.44616	.10507	.55123	24.741	.02298
28	.52052	.12706	.64758	29.066	.02313
32	.59488	.15089	.74577	33.473	.02331

TABLE VII (D)

Evaluation of equation 30 for a counter half-angle of 10 degrees

ΔE	$.03749\ \Delta E$	$.57554\ \ln(78/78-\Delta E)$	$(2/\sigma Z)N_c$	$N_c \propto$	$(2/\sigma Z)N_c/\Delta E$
1	.03749	.00742	.04491	1.0000	.04491
2	.07498	.01495	.08993	2.002	.04497
4	.14996	.03030	.18026	4.014	.04507
8	.29992	.06228	.36220	8.065	.04528
12	.44988	.09615	.54603	12.158	.04550
16	.59984	.13213	.73197	16.299	.04575
20	.74980	.17052	.92032	20.493	.04602
24	.89976	.21164	1.11140	24.747	.04631
28	1.04972	.25594	1.30566	29.073	.04663
32	1.19968	.30393	1.50361	33.481	.04699

TABLE VII (E)

Evaluation of equation 30 for a counter half-angle of 13 degrees

ΔE	$.06250\ \Delta E$	$.95568\ \ell n(78/78-\Delta E)$	$(2/\sigma-Z)N_c$	$N_c\ \propto$	$(2/\sigma-Z)N_c/\Delta E$
1	.06250	.01233	.07483	1.0000	.07483
2	.12500	.02483	.14983	2.002	.07492
4	.25000	.05031	.30031	4.013	.07508
8	.50000	.10341	.60341	8.064	.07543
12	.75000	.15966	.90966	12.156	.07581
16	1.00000	.21941	1.21941	16.296	.07621
20	1.25000	.28314	1.53314	20.488	.07666
24	1.50000	.35143	1.85143	24.742	.07714
28	1.75000	.42498	2.17498	29.066	.07768
32	2.00000	.50467	2.50467	33.471	.07827

TABLE VII (F)

Evaluation of equation 30 for a counter half-angle of 16 degrees

ΔE	$.09408\ \Delta E$	$1.41588\ \ell n(78/78-\Delta E)$	$(2/\sigma Z)N_c$	$N_c\ \alpha$	$(2/\sigma Z)N_c/\Delta E$
1	.09408	.01826	.11234	1.0000	.11234
2	.18816	.03678	.22494	2.002	.11247
4	.37632	.07453	.45085	4.013	.11271
8	.75264	.15321	.90585	8.063	.11323
12	1.12896	.23654	1.36550	12.156	.11379
16	1.50528	.32506	1.83034	16.293	.11439
20	1.88160	.41948	2.30108	20.483	.11505
24	2.25792	.52066	2.77858	24.734	.11577
28	2.63424	.62963	3.26387	29.053	.11657
32	3.01056	.74768	2.75824	33.454	.11745

TABLE VII (G)

Evaluation of equation 30 for a counter half-angle of 20 degrees

ΔE	$.14549\ \Delta E$	$2.13080\ \ln(78/78-\Delta E)$	$(2/\sigma Z)N_c$	$N_c\ \alpha$	$(2/\sigma Z)N_c/\Delta E_c$
1	.14549	.02749	.17298	1.0000	.17298
2	.29098	.05536	.34634	2.002	.17317
4	.58196	.11217	.69413	4.013	.17353
8	1.16392	.23057	1.39449	8.062	.17431
12	1.74588	.35597	2.10185	12.151	.17515
16	2.32784	.48919	2.81703	16.283	.17606
20	2.90980	.63129	3.54109	20.471	.17705
24	3.49176	.78356	4.27532	24.716	.17814
28	4.07372	.94754	5.02126	29.028	.17933
32	4.65568	1.12521	5.78089	33.419	.18065

TABLE VII (H)

Evaluation of equation 30 for a counter half-angle of 24 degrees

ΔE	$.20687\ \Delta E$	$2.92996\ \ln(78/78-\Delta E)$	$(2/\sigma Z)N_c$	$N_c\ \alpha$	$(2/\sigma Z)N_c/\Delta E$
1	.20687	.03780	.24467	1.0000	.24467
2	.41374	.07612	.48986	2.002	.24493
4	.82748	.15423	.98171	4.013	.24543
8	1.65496	.31704	1.97200	8.060	.24650
12	2.48244	.48947	2.97191	12.147	.24766
16	3.30992	.67265	3.98257	16.277	.24891
20	4.13740	.86804	5.00544	20.458	.25027
24	4.96488	1.07741	6.04229	24.696	.25176
28	5.79236	1.30290	7.09526	28.999	.25340
32	6.61984	1.54719	8.16703	33.380	.25522

TABLE VIII

Theoretical relative counting rates of the long counter per unit target thickness at 1960-kev proton energy for various target thicknesses and various counter positions (fresh targets only). Normalized to unity at θ = 5 degrees.

ΔE \ θ°_{eff}	3	5	7	10	13	16	20	24
1	.361	1	1.982	3.996	6.657	9.995	15.390	21.768
2	.361	1	1.980	3.994	6.654	9.988	15.379	21.752
4	.361	1	1.981	3.996	6.656	9.992	15.384	21.796
8	.361	1	1.981	3.993	6.652	9.985	15.371	21.737
12	.360	1	1.982	3.995	6.656	9.990	15.377	21.744
16	.360	1	1.980	3.992	6.650	9.982	15.363	21.720
20	.361	1	1.981	3.995	6.655	9.987	15.369	21.725
24	.360	1	1.981	3.992	6.650	9.980	15.357	21.703
28	.360	1	1.980	3.992	6.651	9.980	15.354	21.695
32	.361	1	1.980	3.992	6.650	9.979	15.348	21.684

APPENDIX C

POSSIBLE SEQUENCES OF CERTAIN DEFINED VALUES OF THE PROTON ENERGY WHICH OCCUR WHEN INTEGRATING OVER THE NEUTRON YIELD CURVE

As the proton energy increases, it passes in succession through the values of E_T, E_c, E_L, $E_T + \Delta E$, $E_c + \Delta E$, and $E_L + \Delta E$ in one of the five possible ways listed below:

I	II	III	IV	V
E_T	E_T	E_T	E_T	E_T
E_c	$E_T + \Delta E$	E_c	$E_T + \Delta E$	E_c
$E_T + \Delta E$	E_c	E_L	E_c	$E_T + \Delta E$
$E_c + \Delta E$	$E_c + \Delta E$	$E_T + \Delta E$	E_L	E_L
E_L	E_L	$E_c + \Delta E$	$E_c + \Delta E$	$E_c + \Delta E$
$E_L + \Delta E$	$E_L + \Delta E$	$E_L + \Delta E$	$E_L + \Delta E$	$E_L + \Delta E$

The inequalities represented in each sequence will tell us under what conditions a particular sequence is applicable.

Case I:

$$\left.\begin{array}{l}\Delta E < E_L - E_c \\ \Delta E > E_c - E_T\end{array}\right) \quad \text{or} \quad \left.\begin{array}{l}E_c < E_L - \Delta E \\ E_c < E_T + \Delta E\end{array}\right)$$

Therefore,

$$E_L - E_c + \Delta E > \Delta E + E_c - E_T$$

$$E_c < \left(\frac{E_L + E_T}{2}\right).$$

For Li(p,n), this gives $E_c < (E_T + 19.85 \text{ kev})$. This limitation on E_c is attained by keeping the counter half-angle less than 45 degrees. However, there is a more strict limitation upon E_c, so that we get:

$$E_c < (E_T + \Delta E) \qquad \text{for} \quad \Delta E < \left(\frac{E_L + E_T}{2}\right) = 19.85 \text{ kev.}$$

$$E_c < (E_L - \Delta E) \qquad \text{for} \quad \Delta E > \left(\frac{E_L + E_T}{2}\right) = 19.85 \text{ kev.}$$

Case II:

$$\left.\begin{array}{l}\Delta E < E_c - E_T \\ \Delta E < E_L - E_c\end{array}\right) \quad \text{or} \quad \left.\begin{array}{l}E_c > E_T + \Delta E \\ E_c < E_L - \Delta E\end{array}\right)$$

$$E_c - E_T + E_L - E_c > 2\Delta E$$

$$\Delta E < \left(\frac{E_L - E_T}{2}\right) = 19.85 \text{ kev.}$$

This is the case for $\theta = 45^\circ$, at which angle $E_c = E_T + 19.85 = E_L - 19.85$ kev. For $\theta < 45^\circ$, $E_c < (E_T + 19.85)$ and $\Delta E < (E_c - E_T)$. For $\theta > 45^\circ$, $E_c > (E_T + 19.85)$ and $\Delta E < (E_L - E_c)$.

Case III:

$\Delta E > (E_L - E_T) = 39.7$ kev for Li(p,n) reaction.

Case IV:

$$\left.\begin{aligned} \Delta E &< E_c - E_T \\ \Delta E &> E_L - E_c \end{aligned}\right) \quad \text{or} \quad \left.\begin{aligned} E_c &> E_T + \Delta E \\ E_c &> E_L - \Delta E \end{aligned}\right)$$

$$E_c - E_T + \Delta E > \Delta E + E_L - E_c$$

$$E_c > \left(\frac{E_L + E_T}{2}\right) = (E_T + 19.85 \text{ kev}).$$

For $\Delta E = \left(\frac{E_L - E_T}{2}\right) = 19.85$ kev, $E_c = E_T + 19.85$ kev, and $\theta = 45^\circ$.
For $\Delta E > \left(\frac{E_L - E_T}{2}\right) = 19.85$ kev, $E_c > (E_T + \Delta E)$, and $\theta > 45^\circ$.

For $\Delta E < \left(\frac{E_L - E_T}{2}\right) = 19.85$ kev, $E_c > (E_L - \Delta E)$, and $\theta > 45^\circ$.

Thus, this case cannot occur for $\theta < 45^\circ$.

Case V:

$$\begin{cases} \Delta E < (E_L - E_T) = 39.7 \text{ kev for Li(p,n)} \\ \Delta E > (E_c - E_T) \\ \Delta E > (E_L - E_c) \end{cases}$$

Therefore,

$$2\Delta E > (E_L - E_T) = 39.7 \text{ kev.}$$

$$\Delta E > \left(\frac{E_L - E_T}{2}\right) = 19.85 \text{ kev.}$$

This is the smallest value of ΔE which may be measured in Case V, and it occurs for $E_c = \left(\frac{E_L + E_T}{2}\right) = E_T + 19.85$ kev, which corresponds to $\theta = 45^\circ$.

Therefore,

For $\theta = 45^\circ$ $\qquad (E_c - E_T) < \Delta E < (E_L - E_T)$

$\qquad 19.85 \text{ kev} < \Delta E < 39.7 \text{ kev.}$

For $\theta < 45^\circ$ $\qquad (E_L - E_c) < \Delta E < (E_L - E_T)$

$\qquad (E_L - E_c) < \Delta E < 39.7 \text{ kev}$

where $(E_L - E_c) > 19.85$ kev.

For $\theta < 30^\circ$ $\qquad 30 \text{ kev} \leq \Delta E < 39.7 \text{ kev.}$

For $\theta = 5^\circ$ $\qquad 39.4 < \Delta E < 39.7 \text{ kev.}$

Summary:

(a) For $\theta < 45°$ and $\Delta E < 19.85$ kev only Cases I and II are possible.

(b) For $\theta < 45°$ and $19.85 < \Delta E < (E_L - E_c)$ only Case I is possible

(c) For $\theta < 45°$ and $19.85 < (E_L - E_c) < \Delta E$ only Cases I and V are possible.

(d) For $\theta < 30°$ and $\Delta E < 30$ kev, only cases I and II are possible.

BIBLIOGRAPHY

1. Hanson, Taschek, and Williams, Revs. Modern Phys. 21, 635 (1949)
2. S. C. Snowden and W. D. Whitehead, Phys. Rev. 90, 615 (1953)
3. T. W. Bonner and J. W. Butler, Phys. Rev. 83, 1091 (1951)
4. E. P. Wigner, Phys. Rev. 73, 1002 (1948)
5. Feshbach, Peaslee, and Weisskopf, Phys. Rev. 71, 145 (1947)
6. A. O. Hanson and J. L. McKibben, Phy. Rev. 72, 673 (1947)
7. Nobles, Day, Henkel, Jarvis, Kutarnia, McKibben, Perry, and Smith, Revs. Sci. Inst. 25, 334 (1954)
8. Hinchey, Stelson, and Preston, Phys. Rev. 86, 483 (1952)
9. E. Segrè, Experimental Nuclear Physics, John Wiley and Sons, (New York, 1953), Vol. I, Part II, Sect. 1.
10. S. K. Allison and S. D. Warshaw, Revs. Modern Phys. 25, 779 (1953)
11. C. B. Madsen and P. Venkateswarlu, Phys. Rev. 74, 1782 (1948)
12. Herb, Snowden, and Sala, Phys. Rev. 75, 246 (1949)

Thesis
D643 Donaghy, C. F. 28803
Determination of target
thickness of thin lithium
targets.

Thesis
D643 Donaghy, C. F. 28803
Determination of target
thickness of thin lithium
targets.

thesD643
Determination of target thickness of thi
3 2768 001 89464 5
DUDLEY KNOX LIBRARY